UCB-NE-4221

Release of Radionuclides from Multiple Canisters in a High Level Waste Repository

J. Ahn, S. Kuo, D. A. Roberts, and P. L. Chambré

Department of Nuclear Engineering
University of California
Berkeley, California 94720

July 1998

The authors invite comments and would appreciate being notified of any errors in the report.

Joonhong Ahn
Department of Nuclear Engineering
University of California
Berkeley, CA 94720
USA

ahn@nuc.berkeley.edu

Table of Contents

1. INTRODUCTION AND BACKGROUND 1

1.1 Results of Previous Study 1
1.2 Objective and Scope of This Study 2

2. REPOSITORY-WIDE TRANSPORT MODEL 3

2.1 Assumed High-Level Waste Characteristics 3
2.2 Geologic Formations and Repository Configuration 4
2.3 The Mass Transport Model 5
2.4 Mathematical Formulation 6
2.4.1 Mass Transport of Radionuclides in Repository 6
2.4.2 Total Mass Existing in the Far Field 9
2.5 Parameter Values 10
2.6 Numerical Results 10
2.6.1 Plutonium 10
2.6.2 Uranium 12
2.7 Summary 16

3. UNCERTAINTIES FOR TOTAL URANIUM MASS IN FAR FIELD 17

3.1 Introduction 17
3.2 Latin Hypercube Sampling 18
3.3 Fixed Parameters 20
3.4 Parameters with Uncertainties 20
3.4.1 Water velocity in the Near-Field Rock 20
3.4.2 Porosity of the Near-Field Rock 20
3.4.3 Porosity of the Bentonite Buffer 20
3.4.4 Diffusion Coefficient of Uranium in Buffer 21
3.4.5 Sorption Distribution Coefficient of Uranium in the Near-Field Rock 21
3.4.6 Sorption Distribution Coefficient of Uranium in Buffer 22
3.4.7 Uranium Solubility 22
3.5 Effect of Number of Realizations 23
3.6 Effect of Distribution Functions 25
3.7 Effect of Near-Field Rock Porosity 28
3.7.1 Cases Considered 28
3.7.2 Results 28
3.8 Summary 31

4. DISCUSSION 33

5. CONCLUSION 35

6. REFERENCES 36

List of Figures

Figure 2.1 Profiles of radionuclide concentration and mass flux in the near field (a) before the radionuclide depletes from the first canister and (b) with an upstream depletion region...5

Figure 2.2 Schematic representation of compartments and diffusive-advective transport path. 6

Figure 2.3 Time of ^{239}Pu depletion from glass logs in compartment *n*. Only the times for compartment 5m, m = 1, 2, Ľ , 40, are plotted, except for compartments 1, through 5. ...11

Figure 2.4 Normalized mass of ^{239}Pu in the far field. 12

Figure 2.5 ^{235}U concentration profiles for 200 compartments. The same profiles will be kept until ^{235}U in the glass log in the first compartment depletes and subsequently for all other compartments. The concentration is a discrete quantity. Each mark represents the concentration at each compartment, although they seem to form continuous curves by overlapping with each other within the same porosity case.....13

Figure 2.6 Time when ^{235}U in the glass log of the *n*-th compartment depletes. 14

Figure 2.7 Effect of the near-fieldrock porosity on mass, $\overline{M}_k$, of uranium isotope *k*, existing in the far field. 15

Figure 3.1 Cumulative probability density function for a normal distribution function sectioned into four equal bins with 0.1% truncation at the high and low ends.....18

Figure 3.2 Density distribution function of a normally distributed function sectioned into four equal bins of approximately 25% each. 19

Figure 3.3 Cumulative probability density Function for sorption distribution coefficient of uranium 21

Figure 3.4 Cumulative probability density function for solubility of uranium 22

Figure 3.5 Difference in frequency distributions obtained by 500 realizations and 4,000 realizations. 23

Figure 3.6 Difference in frequency distributions obtained by 1,000 realizations and 2,000 realizations.....24

Figure 3.7 Cumulative probability density functions of normalized ^{235}U mass in the far field for four different total realizations. 24

Figure 3.8 Frequency curves for the normalized mass of ^{235}U in the far field with combinations of distribution functions shown in Table 3.4 26

Figure 3.9 Cumulative probability density functions for the normalized mass of uranium in the far field for four different combinations of input probability density functions. 27

Figure 3.10 Frequency curves for the normalized ^{235}U mass in the far field with low (case (5)) and normal (case (6a)) near-field rock porosity ranges.....30

Figure 3.11 Frequency curves for the normalized ^{235}U mass in the far field with low (case (6b)) and normal (case (7)) near-field rock porosity ranges.....30

Figure 3.12 Cumulative probability density functions for the normalized mass of uranium in the far field for different rock porosity distributions. 31

List of Tables

Table 2.1 Radionuclides Contained in One HLW Glass Log Generated From Reprocessing of 1 MT of Spent Fuel, at the Beginning of Radionuclide Release From the Glass Log [1]. 3

Table 2.2 Lumped Radionuclide Inventories for Mass Transport Analysis 4

Table 2.3 Assumed Parameter Values for Multiple Glass Log Model 10

Table 3.1 Ranges of Variable Parameter 20

Table 3.2 Assumed Input Parameter Distributions for Observation of the Effect of Realization Number 23

Table 3.3 Summary of Input Parameter Distributions and Statistics of the Resultant Distribution. 25

Table 3.4 Distribution and Ranges for the Study of Host Rock Porosity Range and Statistics of the Resultant Distributions 29

Table 4.1 Summary of Minimum Critical ^{235}U Masses [kg] / Core Radii [cm] for Homogeneous, Spherical, Reflected $U(12)O_2$ + Rock + H_2O Systems [1] 34

Acknowledgments

The research reported herein was supported by the Isolation System Research Program, Radioactive Waste Management Program, Power Reactor and Nuclear Fuel Development Corporation, Japan.

1. INTRODUCTION AND BACKGROUND

1.1 Results of Previous Study

In the previous report [1], an assessment for the feasibility of the autocatalytic criticality phenomena was conducted for vitrified high-level wastes (HLW) from reprocessed fuel of commercial light-water reactors. The study was performed by assuming that the HLW is to be disposed of in fractured granitic rock saturated with water, as is assumed in the Japanese HLW geologic disposal project [2].

To investigate the possibility of the autocatalytic criticality scenario for the vitrified HLW disposed of in a repository, a mathematical model was established for release and transport of actinides from one waste glass log by a hypothetical transport path to an accumulation location. The total accumulation was obtained by superposing the contributions of all 40,000 canisters in the repository. It is thus assumed that all the radionuclides released from all the glass logs in the repository are transported to a single accumulation location, accumulating there, and that each glass log contributes to the accumulation without being influenced by other glass logs. A case was identified where approximately one mole of uranium can be transported to the accumulation location from a single canister with an enrichment of 12%. Therefore, at most a total of 40,000 moles of 12%-enriched uranium can accumulate. This case was found to occur when the solubility of uranium is at an upper bound of the assumed solubility range and the sorption distribution coefficient of uranium is at a lower bound of the assumed range while the solubilities of the precursors to uranium isotopes are at lower bounds and the sorption distribution coefficients of the precursors are at upper bounds. In this case, most of the precursor actinides decay to uranium before they are released from the engineered barrier around a failed waste canister. If the cases are the other way around, i.e., the solubility is lower and the sorption distribution coefficient is greater for uranium, whereas the solubilities are higher and the sorption distribution coefficients are smaller for the precursors, then the total accumulation contributed by all the canisters in the repository is found not sufficiently large to achieve criticality.

A neutronic analysis was performed to identify minimum requirement in a spherical geometry for an autocatalytic criticality event of 12% enriched uranium in water saturated granite rocks [1]. It was found that, with a rock porosity of 0.3 at the accumulation location, over-moderated criticality can be achieved with 12% enriched uranium, and that the critical system can be autocatalytic with system temperature increase if the uranium deposition is heterogeneous.

Thus, starting with the 40,000 vitrified HLW waste glass logs placed in water-saturated geologic formations, cases were identified which lead to supercritical systems that exhibit positive reactivity feedback mechanisms.

In the previous study [1], two things were pointed out:

- With the assumption of independent canister contributions, the total mass of a radionuclide that is released from the repository and exists in the region surrounding the repository (i.e., the far field) is over-estimated. If the radionuclide has a sufficiently long half-life, then significant mass of that radionuclide can survive during the transport between two adjacent waste canisters. The concentration of the radionuclide in the groundwater increases, and so the release of the radionuclide from downstream canisters is inhibited.
- Since geochemical parameters, such as solubilities and sorption distribution coefficients,

have relatively wide ranges of variations, quantifying uncertainties associated with the estimated mass of radionuclide in the far field is of interest.

1.2 Objective and Scope of This Study

Responding to these two points, the objective of this study is twofold. First, to correct the over-estimation due to the conservative assumption of independent canister contributions, an alternate transport model is established by taking into account multiple-canister interference, and the mass of radionuclide existing in the far field is calculated (Chapter 2). Then, using the newly-developed model, we obtain the probability density distribution function of ^{235}U mass existing in the far field based on assumed distribution functions for the input parameters (Chapter 3).

Like previous performance assessments for the radiological impact of geologic repositories [3, 4], the present study on the performance assessment for the criticality safety of geologic repositories also consists of three parts: (1) development of a deterministic model for a performance measure, (2) a statistical analysis for uncertainties associated with the performance measure obtained by the established deterministic model, and (3) judgement of repository performance by comparing the obtained value of the performance measure (with the uncertainties) with the safety criterion.

In the first part, which is set out in Chapter 2, a deterministic model is established for estimating the total mass of radionuclides of interest in the far field. With the model, observations are made of mechanisms that govern the radionuclide transport in the repository region and mechanisms how the repository transport mechanisms affect the total mass of radionuclides existing in the far field. Of particular interest in this study is the release of ^{239}Pu, ^{235}U, and ^{238}U from the repository. As we see later in Chapter 2, due to its relatively short half-life, the release of ^{239}Pu from the repository to the far field is negligibly small. The analysis is simplified by focusing on the transport of ^{235}U. Because ^{235}U is the principal fissile material in the configuration considered in this study, we choose the total mass of ^{235}U existing in the far field as the performance measure for the repository safety in the aspect of criticality safety.

In the second part, which is described in Chapter 3, a statistical analysis is performed to quantify the uncertainties associated with the performance measure, i.e., the total mass of ^{235}U existing in the far field, with probability distribution functions assumed for following model input parameters: the water velocity, the porosity of the near-field rock, the porosity of the buffer, the uranium solubility, the uranium sorption coefficients in the buffer and the near-field rock regions, and the diffusion coefficient in the buffer region. Following an assumed probability distribution function for each parameter, values for the parameters are sampled, and the mass of ^{235}U in the far field is calculated. By repeating this procedure, a probability density distribution for the mass of ^{235}U in the far field is obtained. The Latin Hypercube Sampling (LHS) method [5] is employed because the number of realizations required for a statistically significant analysis is notably reduced [6, 7]. A computer program developed by Iman and Shortencarier [8] is used in this study.

In the third part, set out in Chapter 4, the performance measure for the criticality safety, i.e., the ^{235}U mass existing in the far field with its uncertainty (or, an error bar) is compared with the criterion for criticality safety, i.e., the minimum masses required for criticality obtained in the previous study [1].

2. REPOSITORY-WIDE TRANSPORT MODEL

2.1 Assumed High-Level Waste Characteristics

In **Table 2.1** [1], the inventories of radionuclides in 1 MT of spent fuel from PWR initially enriched at 4.5% with a burnup of 45,000 MWD/MT are given, and the inventories of radionuclides in HLW arising from 1 MT of the same spent fuel are calculated by ORIGEN2 code [9]. The spent fuel is stored for four years of cooling before reprocessing. At reprocessing, it is assumed that 99.33% of plutonium and 99.85% of uranium are recovered. Minor actinides, such as ^{245}Cm, ^{241}Am, ^{237}Np, and ^{243}Am, will not be recovered by reprocessing. It is assumed that HLW from 1 MT of PWR spent fuel is vitrified with borosilicate glass contained in one waste canister. The vitrified HLW is stored for fifty years before emplacement in the repository. The waste glass is assumed to start radionuclide release a thousand years after the emplacement. The origin of the time (t = 0) is counted from the moment when radionuclide release from glass logs begins, i.e., 1054 years after the discharge of spent fuel from a reactor.

The previous study [1] shows that the case of concern occurs when the solubility of uranium is at the upper bound of the assumed solubility range and the sorption distribution coefficient of uranium is at the lower bound of the assumed range of its sorption distribution coefficient while the solubilities of the precursors to uranium isotopes are at the lower bounds and the sorption distribution coefficients of the precursors are at the upper bounds. In this case,

Table 2.1 Radionuclides Contained in One HLW Glass Log Generated From Reprocessing of 1 MT of Spent Fuel, at the Beginning of Radionuclide Release From the Glass Log [1].

	Nuclide	Half-life	Inventory			
			HLW		Spent fuel	
		[yr]	[mol]	[kg]	[mol]	[kg]
	Pu-240	6.57E+3	2.00E-1	4.8E-2	2.86E+1	7.2
	U-236	2.34E+7	5.59E-2	1.3E-2	3.73E+1	8.8
√	Cm-245	9.30E+3	7.55E-3	1.8E-3	7.55E-3	1.8E-3
	Am-241	4.58E+2	2.82E-1	6.8E-2	2.82E-1	6.8E-2
	Np-237	2.14E+6	4.02	0 95	4.02	0 95
√	U-233	1.62E+5	1.24E-3	2.9E-4	8.27E-1	1.9E-1
	Pu-242	3.76E+5	1.80E-2	4.4E-3	2.57	6.5E-1
	U-238	4.46E+9	5.83	1.4	3.87E+3	9.3E+1
	U-234	2.45E+5	1.11E-2	2.6E-3	7.40	1.7
	Am-243	7.37E+3	4.86E-1	1.2E-1	4.86E-1	1.2E-1
√	Pu-239	2.44E+4	2.54E-1	6.1E-2	3.63E+1	9.1
√	U-235	7.04E+8	7.00E-2	1.6E-2	4.67E+1	1.1E+1
	B	———	1.00E+3	5.7E+1	———	———

99.85% of U and 99.33% of Pu are assumed to be recovered at the reprocessing stage. Calculated by ORIGEN2 code [9]. B_2O_3 content is assumed to be 14 wt%. Total weight of borosilicate glass is assumed to be 405 kg. Notice that inventories for Cm, Am, and Np isotopes in HLW are the same those in spent fuel. Nuclides with √ mark are fissile; others are categorized as neutron absorbers (or poisons).

most of the precursor actinides decay to uranium before they are released from the engineered barrier around a failed waste canister. Approximately one mole of 12%-enriched uranium is supplied to the accumulation location 1,000m away from a canister .

Based on this result, among the radionuclides considered in the previous study [1] and shown in **Table 2.1**, we focus on three radionuclides in this study: ^{239}Pu, ^{235}U and ^{238}U (see **Table 2.2**). ^{239}Pu is kept despite its relatively short half-life because it is an important fissile radionuclide, but later in this chapter, we will observe that most of ^{239}Pu in one glass log decays to ^{235}U within the vicinity of the glass log. Accumulation of ^{236}U, ^{234}U, and ^{233}U was found to be negligible in the previous study. Therefore, for an analysis of uranium transport, a simplification is done by lumping the initial masses of the precursors with those of ^{235}U and ^{238}U, and by neglecting ^{236}U, ^{234}U, and ^{233}U. For example, ^{243}Am and ^{239}Pu will decay to ^{235}U. With the inventories given in **Table 2.1**, the mass of ^{235}U available per canister is calculated as $0.486 + 0.254 + 7.00 \times 10^{-2} = 0.810$ mol. Similarly, $1.80 \times 10^{-2} + 5.83 = 5.85$ mol for ^{238}U is obtained. With these numbers, the fissile-isotope fraction in total uranium mass, or the enrichment, defined as $^{235}\text{U}/(^{238}\text{U} + ^{235}\text{U})$, can be calculated as $(0.810)/(5.85 + 0.810) = 0.12$, or 12%.

Table 2.2 Lumped Radionuclide Inventories for Mass Transport Analysis

Nuclide	Lumped inventory in one HLW glass log [mol]	Lumped radionuclides
Pu-239	7.40E-1	Am-243
U-235	8.10E-1	Am-243, Pu-239
U-238	5.85	Pu-242

2.2 Geologic Formations and Repository Configuration

We choose granite as host rock, based on the previous performance assessment study [2]. A repository is assumed to be built under the water table [2]. The present analysis is to be made under the assumption that any void spaces in the repository and the surrounding host rock are fully saturated with water.

A detailed repository design is yet to be determined. It is assumed that a total of 40,000 waste canisters would be disposed of by placing them in a two dimensional array fashion. Roughly 100 m^2 is allocated for a waste canister [2], and the repository has dimensions of 2,000 m × 2,000 m.

For an engineered barrier system (EBS) around the waste canister, a thick carbon-steel overpack and a bentonite-filled buffer region is assumed between the waste solid and the host rock. The lifetime of an overpack is conservatively assumed to be 1,000 years. In the early stage of the first 1,000 years after the emplacement of the waste canister, the heat generation from a canister would rapidly decrease, and the temperature in the repository would settle down to the ambient temperature [10]. It is assumed that the bentonite buffer would be fully saturated by groundwater by then.

Once the overpack loses its integrity, the waste glass starts to dissolve by porewater in the bentonite buffer, together with the fissile and other materials contained in the glass log. Bentonite is expected to have a hydraulic conductivity more than three orders of magnitude smaller than that of the surrounding host rock [2]. Bentonite swells by water uptake, and seals intersecting fractures. Due to pyrite in bentonite and the carbon-steel overpack, the porewater in

the engineered-barrier region is assumed to be in a reducing state. The hydrological and geochemical condition within the engineered barriers is assumed constant in time. Under a reducing environment, the concentrations of uranium and actinides in the porewater at the waste-glass dissolution location are limited by their solubilities. Radionuclides are assumed to be transported through the porewater in the bentonite buffer region by molecular diffusion.

2.3 The Mass Transport Model

If the half-life is sufficiently long, the radionuclide released from the upstream glass logs will remain in the water stream, and the concentration in the water stream will increase as the water stream passes by additional glass logs. **Figure 2.1 (a)** qualitatively illustrates the concentration profile at some early time t_1 in the near field rock. Because the mass flux from a glass log to the flowing groundwater in the near-field rock is determined by the concentration difference between the glass-log surface and the water stream, the mass flux is smaller for the downstream glass logs than for the upstream glass logs. Here, it is assumed that the concentration on the glass-log surface is constant at its solubility.

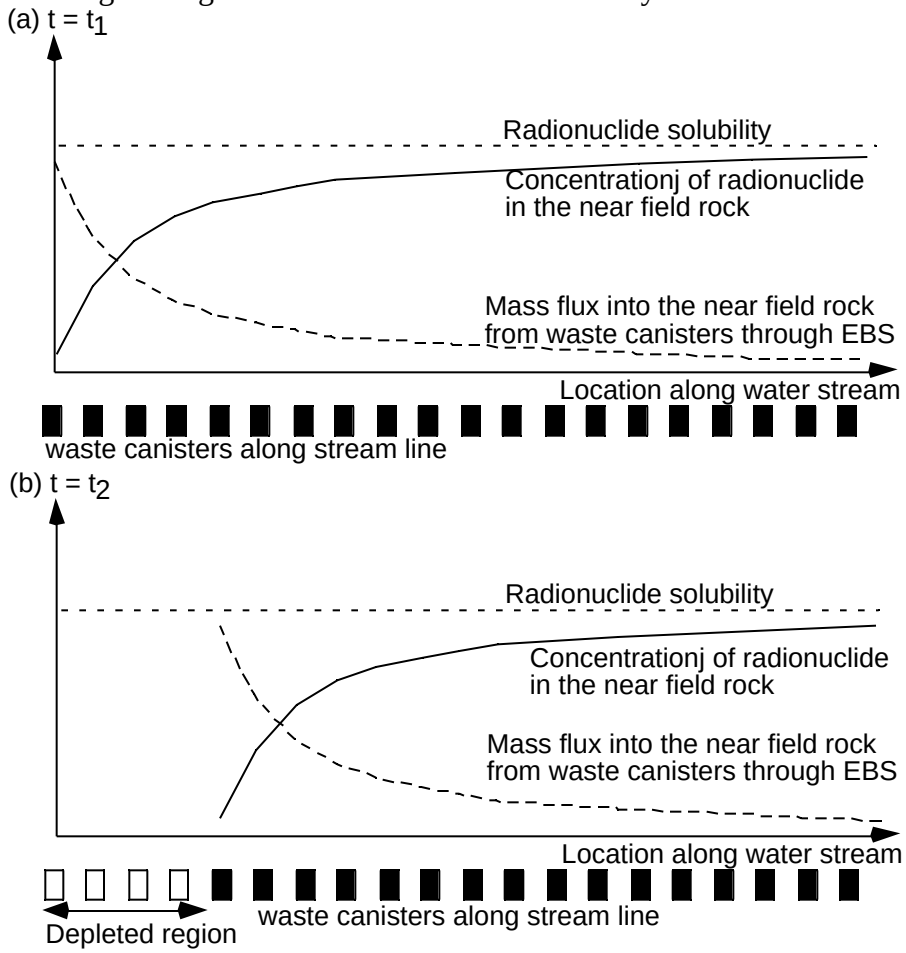

Figure 2.1 Profiles of radionuclide concentration and mass flux in the near field (a) before the radionuclide depletes from the first canister and (b) with an upstream depletion region

As the radionuclide diffuses through the buffer, the radionuclide mass in the waste glass decreases by decay and diffusion. The radionuclide inventory in the waste glass is depleted faster from the upstream canisters than it is from the downstream canisters due to the steeper concentration gradient on the upstream side of the repository.

Figure 2.1(b) illustrates the depletion of the radionuclide mass in the upstream canisters at some later time, t_2. At most upstream side of the repository, the concentration gradient is the largest because the water flowing into this region of the near-field rock contains no radionuclide. Therefore, the mass flux is the largest there and the complete depletion would occur the earliest for the first canister. After the first canister depletes completely, then the second canister is exposed to the highest mass flux among the remaining waste canisters. Thus, the radionuclide mass in waste canisters depletes from the upstream side toward the downstream.

2.4 Mathematical Formulation

2.4.1 Mass Transport of Radionuclides in Repository

To take into account the effects of interference among multiple glass logs, we develop a model, depicted in **Figure 2.2**, where a row of glass logs is divided into compartments, each containing a glass log, the bentonite buffer around the glass log, and the near-field host rock. The compartment has an areal extent of $d \times d$, where d [m] is the pitch between two adjacent glass logs.

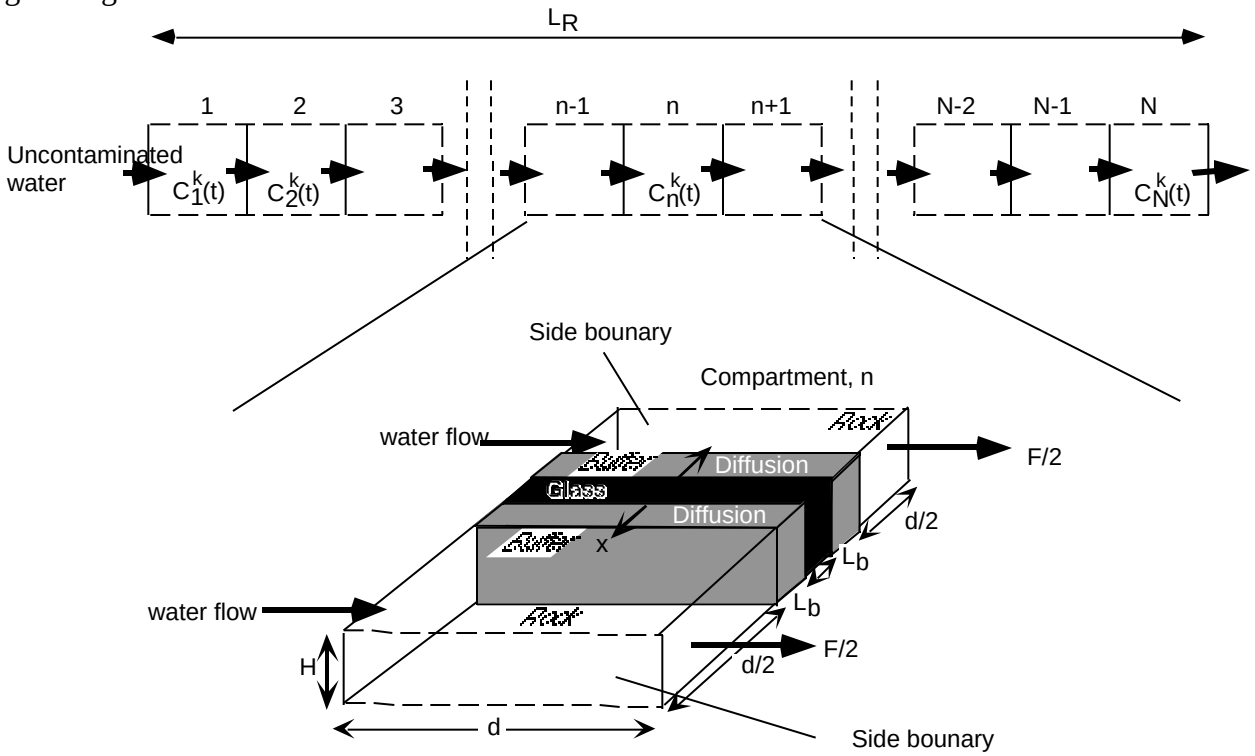

Figure 2.2 Schematic representation of compartments and diffusive-advective transport path.

The rock and the buffer are assumed to be homogeneous porous media. Sorption equilibrium between the solid phase and the porewater phase is assumed. The steel overpack

between the buffer and the glass log is neglected in this analysis.

We transform the cylindrical waste form into a slab geometry with the same interfacial area. As is depicted in **Figure 2.2,** the slab source is assumed to have a width *d*. Between the slab source and the near-field rock, there are assumed to be the bentonite region on both sides of the slab source. The bentonite region has the thickness of L_b. To make the surface area of both sides of the slab equal to the surface area, *S,* of the original cylindrical glass log, the hypothetical slab height *H* is determined as

$$2dH = S. \tag{1}$$

The water flow rate, *F* [m^3/yr], the volumetric flow rate of water through the interface between two adjacent compartments, is defined as:

$$F = vHd\varepsilon_p, \tag{2}$$

where *v* [m/yr] is the pore velocity of groundwater. ε_p is the porosity of rock. In actuality, the groundwater velocity, *v*, varies with the location in the rock. But, in this analysis, the velocity is assumed to be constant spatially and temporally.

Mass balance equations are obtained for radionuclide *k* existing in the rock and for radionuclide *k* remaining in the glass log.

In the glass log,

$$\frac{dm_k^n(t)}{dt} = -\lambda_k m_k^n(t) - Q_k^n(t), \quad t > 0, \ n = 1, 2, ..., N, \tag{3}$$

where $m_k^n(t)$[mol] is the mass of radionuclide *k* in the glass log in the *n*-th compartment. $Q_k^n(t)$ [mol/yr] is the release rate of radionuclide *k* from the bentonite buffer to the near-field rock. *N* is the total number of compartments. λ_k [yr^{-1}] is the decay constant of radionuclide *k*.

For the near field rock region, two assumptions are made. First, the concentration of radionuclide *k* is assumed to be $C_k^n(t)$[mol/m^3] everywhere in the pore water of the near-field rock of compartment *n* located relative to the upstream side of the repository. The second assumption is no mass transport through the side boundaries of the compartment. The side boundaries coincide with the mid-plane between two adjacent rows of waste forms. If each waste form releases radionuclides equally, no mass transport occurs through the mid-planes due to zero concentration gradient perpendicular to the mid-planes. The governing equation for $C_k^n(t)$ is written as

$$\alpha_{e(k)} V \frac{dC_k^n(t)}{dt} = -\lambda_k V \alpha_{e(k)} C_k^n(t) + FC_{k-1}^n(t) - FC_k^n(t) + Q_k^n(t), C_k^0 = 0, \ t > 0, \ n = 1, 2, ..., N.. \tag{4}$$

V [m^3] is the volume of the near-field rock in a compartment. Effects of precursors are neglected in this formulation. $\alpha_{e(k)}$ is the capacity factor for element *e*, and is defined by

$$\alpha_{e(k)} = \varepsilon_p + \rho_r (1 - \varepsilon_p) K_{dp}^e, \tag{5}$$

where ρ_r [kg/m^3] is the density of the porous rock matrix, and K_{dp}^e [m^3/kg] is the sorption distribution coefficient of element *e* for the rock matrix. Subscript *e(k)* indicates that radionuclide *k* is an isotope of element *e*.

Equations (3) and (4) are solved subject to the initial conditions:

$$C_k^n(0) = 0, \ n = 1, 2, ..., N, \tag{6}$$

and $$m_k^n(0) = M_{k(o)} \quad n = 1, 2, ..., N, \tag{7}$$

where $M_{k(o)}$ [mol] is the initial mass of radionuclide *k* in a glass log. Here, $M_{k(o)}$ is obtained by lumping the initial masses of the precursors with that of radionuclide *k* as shown in **Table 2.2.** $M_{k(o)}$ is assumed to be identical for all the compartments.

Bentonite is expected to have a hydraulic conductivity about three orders of magnitude smaller than that of the host rock. Radionuclides released from the waste glass are assumed to diffuse through the bentonite buffer into the near-field rock. The diffusion of radionuclides through the bentonite region is considered to be one-dimensional. Radioactive decay during the diffusion is included. Considering that the water velocity in the surrounding rock is as small as 1 m/yr, and that we are primarily interested in the mass transport in the time frame of 100,000 years or longer, we assume that the concentration profile in the buffer is approximated by a quasi-steady state solution. Then, the concentration, $N_k^n(x;t)$, of radionuclide *k* in the buffer is governed by the following equation:

$$D_{e(k)} \frac{d^2 N_k^n}{dx^2} - K_{e(k)} \lambda_k N_k^n = 0, \quad n = 1, 2, \ldots, N, \quad 0 < x < L_b, \tag{8}$$

where $D_{e(k)}$ is the molecular diffusion coefficient [m^2/yr] for element *e*. Equation (8) describes quasi-steady state balance between diffusion and radioactive decay. The concentration $N_k^n(x;t)$ has time-dependency because of the boundary condition. At the buffer/rock interface, we impose the following boundary condition:

$$N_k^n(L_b;t) = C_k^n(t), \quad n = 1,2,\ldots, N, \; t > 0. \tag{9}$$

By (9), it is assumed that the concentration profile in the buffer follows the change in the concentration at the interface and a quasi-steady state with that interface concentration is reached instantaneously.

At the waste glass surface, the following boundary condition is imposed:

$$N_k^n(0;t) = N_e^* \gamma_k^n, \quad n = 1,2,\ldots, N, \; t > 0, \tag{10}$$

where N_e^* is the solubility of element *e*. The factor, γ_k^n, is the solubility appropriation for isotope *k*, if element *e* has multiple isotopes. In our case, ^{235}U and ^{238}U share the uranium solubility. Because the half-lives of these uranium isotopes are very long, the solubility appropriation factors are approximated by the following constants:

$$\gamma_{238}^n = \frac{M_{238(0)}}{M_{238(0)} + M_{235(0)}}, \quad \gamma_{235}^n = \frac{M_{235(0)}}{M_{238(0)} + M_{235(0)}}, \quad n = 1,2,\ldots N, \tag{11}$$

where they are assumed constant with time and identical for all the compartments.

The retardation coefficient, $K_{e(k)}$, is defined as:

$$K_{e(k)} = 1 + \frac{\rho(1 - \varepsilon)}{\varepsilon} K_d^e, \tag{12}$$

where ρ [kg/m^3] and ε are the density and the porosity of the bentonite, respectively.

The solution to (8) subject to (9) and (10) is obtained as

$$N_k^n(x;t) = \frac{\gamma_k^n N_e^* \sinh\left[(L_b - x)\sqrt{\frac{\lambda_k K_{e(k)}}{D_{e(k)}}}\right] + C_k^n(t)\sinh\left[x\sqrt{\frac{\lambda_k K_{e(k)}}{D_{e(k)}}}\right]}{\sinh\left[L_b\sqrt{\frac{\lambda_k K_{e(k)}}{D_{e(k)}}}\right]},$$

$$0 \le x \le L_b, t > 0,\ n = 1,2,\ldots,N. \tag{13}$$

$N_k^n(x;t)$ is not defined at $t = 0$ because of the quasi-steady state assumption. $Q_k^n(t)$ in eq. (4) is, then, computed by obtaining the concentration gradient at the bentonite/rock interface from eq. (13) and multiplying it by the porosity of the bentonite, the diffusion coefficient, and the surface area of the interface, as

$$Q_k^n(t) = \frac{S\varepsilon\sqrt{D_{e(k)}\lambda_k K_{e(k)}}}{\sinh\left[L_b\sqrt{\frac{\lambda_k K_{e(k)}}{D_{e(k)}}}\right]}\left[\gamma_k^n N_e^* - C_k^n(t)\cosh\left[L_b\sqrt{\frac{\lambda_k K_{e(k)}}{D_{e(k)}}}\right]\right] \quad 0 < t < t_k^n, n = 1,2,\ldots,N, \tag{14}$$

where t_k^n is the time when radionuclide k depletes completely from the glass log in compartment n. After t_k^n, $Q_k^n(t)$ is set to equal to zero.

2.4.2 Total Mass Existing in the Far Field

The region outside of the repository region is defined here as the far field.

From the downstream side of the repository, i.e., from compartment N, radionuclide k is released into the far field. We consider the mass $\overline{M}_k(t)$ of radionuclide k existing in the far field at time t, as the performance measure for the criticality safety because that can be considered as the theoretical maximum for the mass of radionuclide k that can accumulate in a single location. For a fissile radionuclide such as ^{235}U, the most conservative assumption for criticality safety assessment is that all of the radionuclide released from the repository region to the far field accumulates at a single location. Because the radionuclide that is released from the repository region is dispersed in the far field, the situation considered will never happen, but the mass of accumulated radionuclide in a single location should always be smaller than the total mass existing in the far field. To quantify the actual accumulation, we must know the detailed mechanisms and conditions for the mass transport and accumulation in the far field.

To calculate the mass, $\overline{M}_k(t)$, of all radionuclide k, existing in the far field, the mass balance equation (15) can be written. Radioactive decay loss is taken into account.

$$\frac{d\overline{M}_k}{dt} = -\lambda_k \overline{M}_k + FC_k^N(t),\ t > 0, \tag{15}$$

subject to $\overline{M}_k(0) = 0$. See **Figure 2.7**.

Equations (3) (4), and (15) are solved numerically by discretizing time. At each time step, C_k^n and m_k^n are calculated for all N compartments. Calculation for m_k^n of each compartment continues until it becomes zero. $\overline{M}_k(t)$ is calculated by using the value of $C_k^N(t)$ obtained at each time step. The calculation for $m_k^n(t)$ is continued until t_k^n when it becomes zero. After t_k^n, $m_k^n(t)$ is set to be zero.

2.5 Parameter Values

Table 2.3 shows the parameter values used in the calculations in the rest of this chapter. Values for solubilities and sorption distribution coefficients are the same as those selected for case (b) in the previous study [1]. Three values are selected to observe the effect of the near-field rock porosity.

Table 2.3 Assumed Parameter Values for Multiple Glass Log Model

Areal extent of the compartment, $d \times d$	10 m × 10m	F
Number of compartments, N	200	F
Thickness of the bentonite buffer, L_b	0.98 m #	F
Surface area of the waste glass, S	2.10 m^2	F
Hypothetical compartment height, $H = S/2d$	0.105 m	F
Porosity of the bentonite region, ε	0.3	V
Density of the bentonite region, ρ	2100 kg/m^3	F
Porosity of the host rock, ε_p	0.01, 0.1, 0.5	V
Density of the host rock, ρ_p	2600 kg/m^3	F
Diffusion coefficient in the bentonite, $D_{e(k}$	3×10^{-2} m^2/yr	V
Water pore velocity across compartment boundary, v	1.0 m/yr	V
Sorption distribution coefficient of uranium in bentonite, K_d^U	0.1 m^3/kg #	V
Sorption distribution coefficient of uranium in rock, K_{dp}^U	0.0001 m^3/kg #	V
Solubility of uranium, N_U^*	10^{-5} mol/m^3 #	V
Sorption distribution coefficient of plutonium in bentonite, K_d^{Pu}	10 m^3/kg #	—
Sorption distribution coefficient of plutonium in rock, K_{dp}^{Pu}	25 m^3/kg #	—
Solubility of plutonium, N_{Pu}^*	10^{-7} mol/m^3 #	—
Initial mass of ^{235}U in a glass log, M_{235}^o	0.81 mol *	F
Initial mass of ^{238}U in a glass log, M_{238}^o	5.83 mol *	F
Initial mass of ^{239}Pu in a glass log, M_{238}^o	0.74 mol *	—
Isotopic appropriation factor for ^{235}U, γ_{235}	0.122	F
Isotopic appropriation factor for ^{238}U, γ_{238}	0.878	F

* : same as those in **Table** 2.2; #: from Ref. [2]. V: Variables with uncertainties, F: Fixed (see Chapter 3)

2.6 Numerical Results

2.6.1 Plutonium

Figure 2.3 shows the numerical results for the time for ^{239}Pu to disappear from the waste glass in compartment n. ^{239}Pu in the glass log in compartment 1 depletes at 476,070 yr. At 476,079 yr, ^{239}Pu depletes completely from the glass log in the second compartment. At 476,080 yr, ^{239}Pu depletes completely from the glass logs in the rest (from the third to the 200-th compartment) simultaneously.

Due to its short half-life and strong sorption to the bentonite and the rock, most ^{239}Pu

released from the buffer decays in the near-field rock of the same compartment before it reaches the next compartment. The ^{239}Pu concentration in the water coming from the upstream compartment remains relatively low, and so release of ^{239}Pu from downstream canisters is not affected significantly by the upstream compartments. Thus, the time of ^{239}Pu depletion for the compartments $n \geq 3$ is identical. However, for the first and second compartments, due to uncontaminated water flowing into the first compartment, the concentration gradient at the buffer/rock interface is maintained higher than that in the other compartments, resulting in slightly earlier depletion.

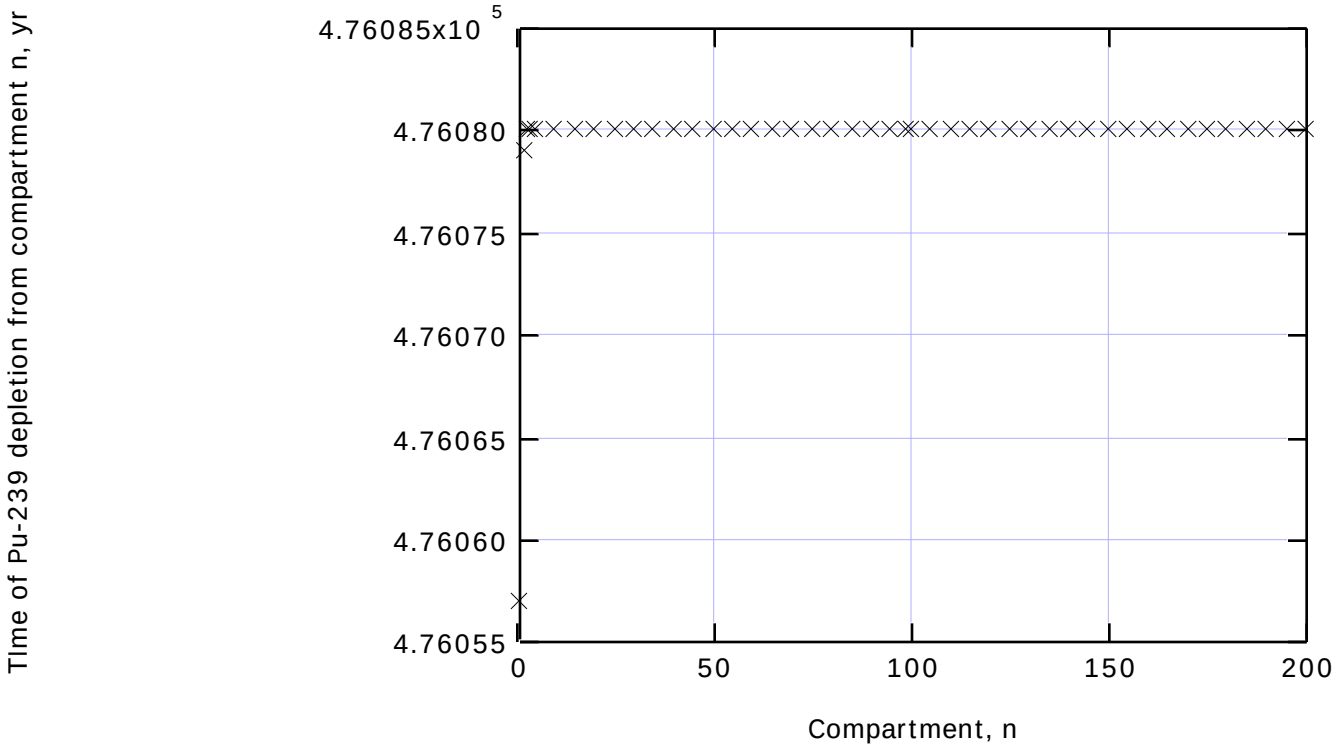

Figure 2.3 Time of ^{239}Pu depletion from glass logs in compartment *n*. Only the times for compartment 5m, m = 1, 2, …, 40, are plotted, except for compartments 1, through 5.

Figure 2.4 shows the total mass, $\overline{M}_{239}$, of ^{239}Pu in the far field, normalized by the total mass, $N\ M_{239(o)}$, of ^{239}Pu that initially exists in the glass logs in the repository. The theoretical maximum of the normalized mass in the far field is unity. The figure shows that only less than 10^{-9} of the initially available ^{239}Pu in the repository can exist in the far field. ^{239}Pu is released from the repository until 476,080 year when ^{239}Pu depletes from 198 glass logs in the repository (see **Figure 2.3**). Therefore, the normalized mass in the far field increases by that time and decreases thereafter due to radioactive decay.

Observations in Figure 2.4 indicate that neighboring glass logs have negligible effects on the release of ^{239}Pu from the canister of interest. This means that most of ^{239}Pu released from a glass log decays in the near field rock of the same compartment before it is transferred to the adjacent compartment. Thus, the transport distance of ^{239}Pu in the repository region is observed to be less than the spacing between two adjacent glass logs. Considering the short transport distance observed in **Figure 2.3**, most of ^{239}Pu in the far field exists in the vicinity of the

repository boundary. Therefore, it is concluded that the accumulation of ^{239}Pu, even if it occurs, will be negligibly small. This allows us to simplify the analysis for transport of uranium isotopes. In the following section, the masses of precursors, ^{243}Am and ^{239}Pu, are lumped with that of ^{235}U, and only two major uranium isotopes, ^{235}U and ^{238}U, will be considered as two single radionuclides with no precursors.

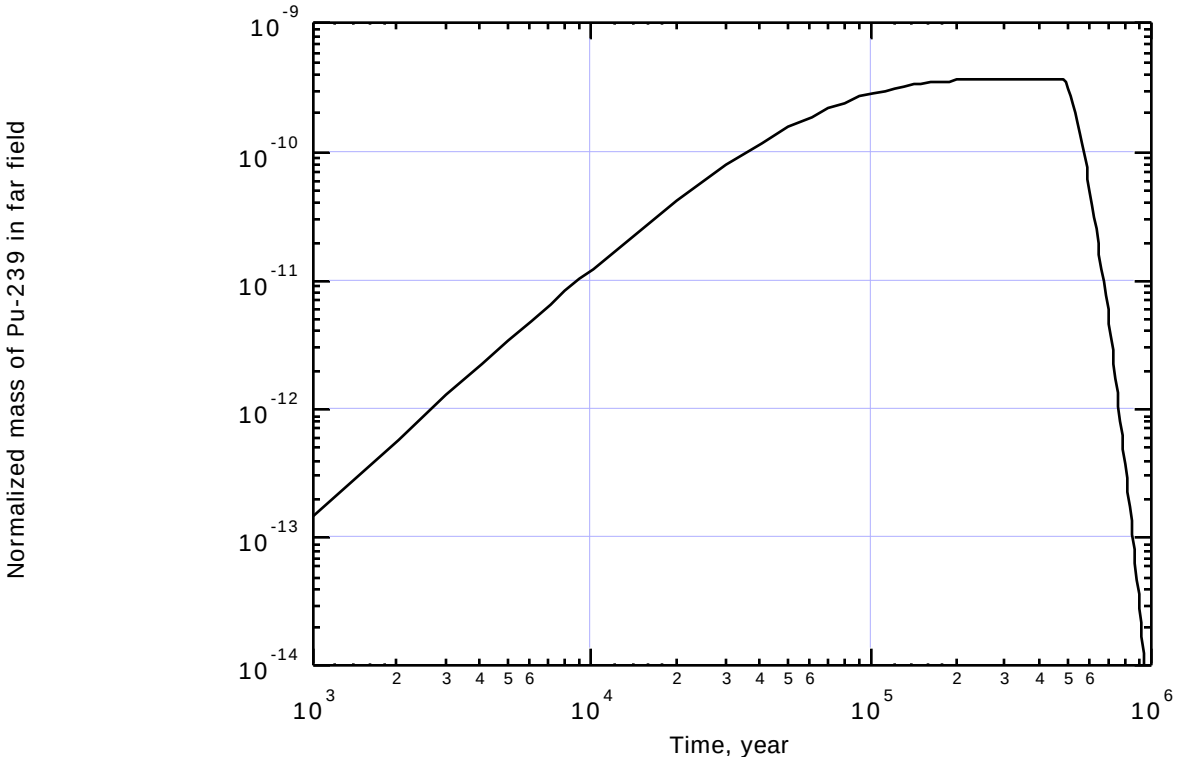

Figure 2.4 Normalized mass of ^{239}Pu in the far field.

2.6.2 Uranium

Figure 2.5 shows the steady-state concentration profiles of ^{235}U for 200 compartments placed in a row. Three curves are plotted for three different porosities of the near-field host rock. The concentrations in the near field changes with time at early times. Eventually, by eq. (3), the rate of change of the mass of uranium isotope *k* in compartment *n* becomes zero, and a steady state is reached at compartment *n*. The time when a steady state is reached is earlier for a smaller rock porosity in the near field.

To understand the mechanisms, let us take a look at the mass transfer in compartment 1 (see Figure 2.3). Since uncontaminated water flows into this compartment and the concentration at the waste glass surface is limited by the nuclide solubility, the mass flux, $Q_k^1(t)$, from the buffer, which is determined by the concentration gradient in the buffer at the rock interface, is approximately the same for different rock porosities. With a smaller rock porosity in the near field, the concentration in water in the near-field rock pores increases more with approximately the same $Q_k^1(t)$. The concentration builds up as the water passes through more compartments, and the flux $Q_k^n(t)$ from the buffer decreases as *n* increases. Eventually, the concentration becomes unchanged from one compartment to another because the total amount of radionuclide

coming from the buffer and from the previous compartment balances with those lost by radioactive decay and by transfer to the next compartment. Thus, the concentration becomes unchanged at a certain compartment *n'* and thereafter. The compartment number *n'* increases with a greater rock porosity in the near field.

The steady-state concentration profile is kept until the radionuclide completely vanishes from the glass log in compartment 1. After the depletion, the concentration changes with time at each compartment, but it reaches temporarily a steady state again. The length of time necessary for a steady state to be restored is approximately the same as the time required for the previous steady state to be reached. The established steady state concentration profile is exactly the same as the one for the previous steady state, except that the profile is shifted by one compartment (Figure 2.2). Depletion will happen for one compartment after another from compartment 1 to *N*. The behavior is the same for ^{238}U.

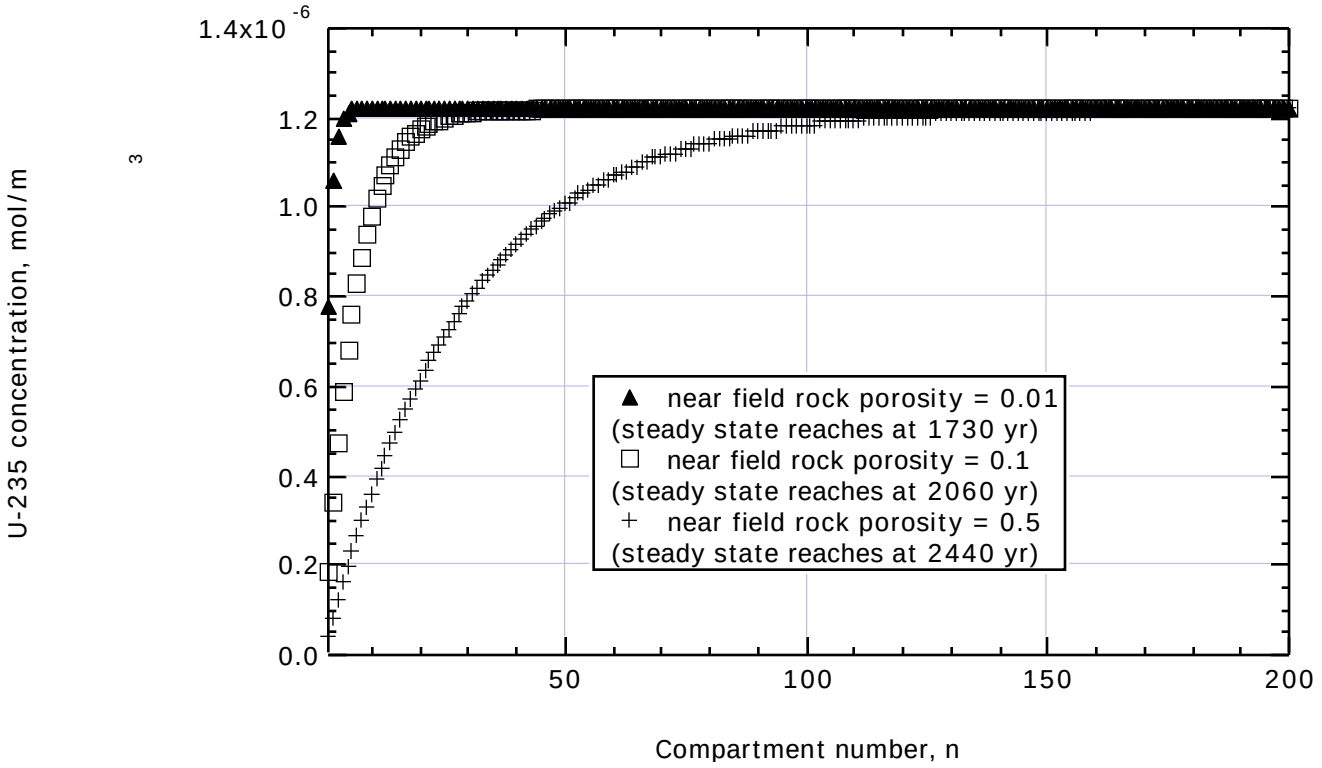

Figure 2.5 **^{235}U concentration profiles for 200 compartments. The same profiles will be kept until ^{235}U in the glass log in the first compartment depletes and subsequently for all other compartments. The concentration is a discrete quantity. Each mark represents the concentration at each compartment, although they seem to form continuous curves by overlapping with each other within the same porosity case.**

Figure 2.6 shows the time when ^{235}U in the glass log of the *n*-th compartment is depleted for three different rock porosities. With a greater near-field rock porosity, more radionuclide can be transported through the near-field rock, and so depletion occurs earlier at any compartment. ^{235}U in the glass log in the first compartment depletes approximately in 400 million years. If the multiple-canister interference was not considered, ^{235}U in all glass logs in the repository would deplete simultaneously at that time. However, due to the interference, it takes a much longer

time for ^{235}U to be depleted in the downstream glass logs. From the glass log in the 200-th compartment, ^{235}U depletes at 1.4 billion years for the near-field rock porosity of 0.5, 2.8 billion years for 0.1, and 5 billion years for 0.01. Thus, it is observed that the interference delays the release of uranium from the downstream glass logs significantly.

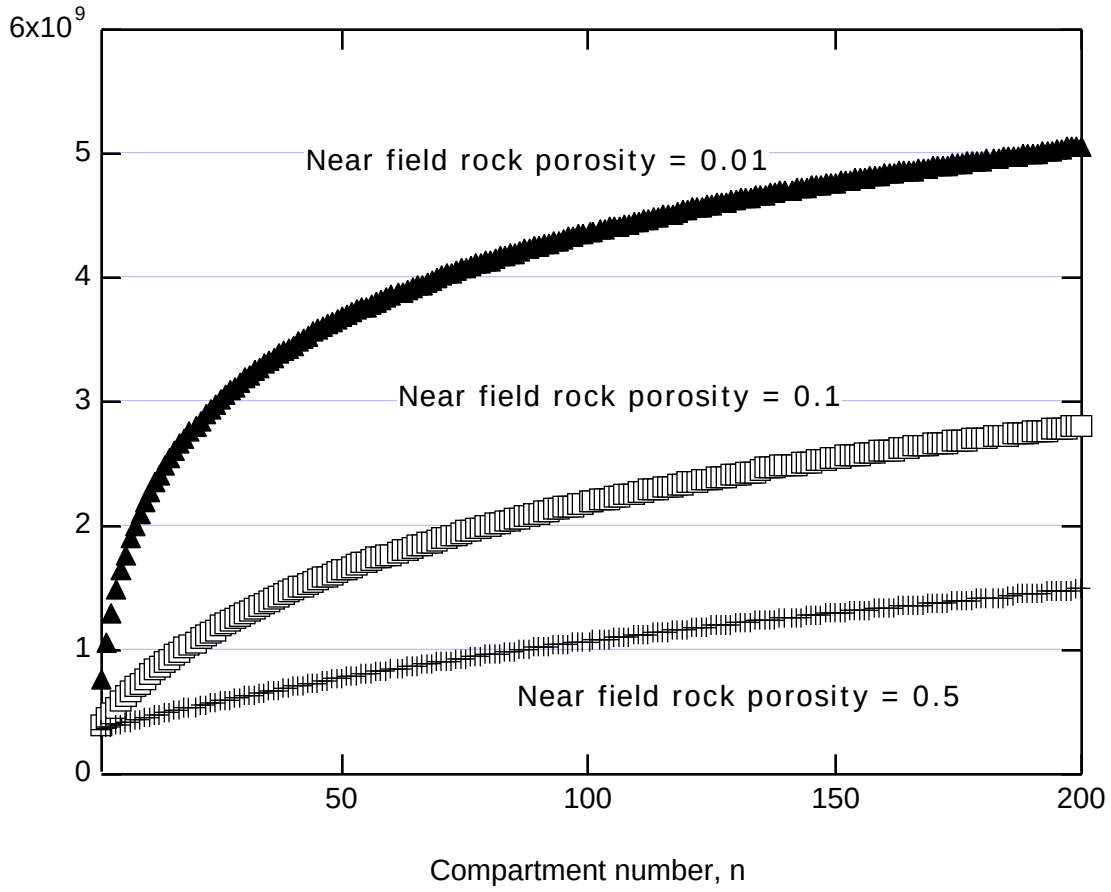

Figure 2.6 Time when ^{235}U in the glass log of the *n*-th compartment depletes.

Figure 2.7 shows the masses, $\overline{M}_k$, of ^{235}U and ^{238}U existing in the far field, normalized by the total initial masses, $NM_{k(o)}$, in the repository for k = 235 and 238 as a function of time. The enrichment, defined as the ratio of the mass of ^{235}U in the far field to the mass of total uranium in the far field, is also plotted in the figure. The enrichment curve is found to be identical for different porosities.

The near-field rock porosity has significant influence on the total mass of uranium in the far field. With the near-field porosity of 0.5, about a quarter of the uranium initially existing in the repository, is observed to remain in the far field for 1 billion years. As the porosity decreases, so does the total mass of uranium. With the porosity of 0.01, the total uranium mass cannot exceed 1% of the total initial mass in the repository before 1 billion yr. The normalized mass of ^{235}U starts to deviate from that of ^{238}U due to its shorter half-life. As shown in **Figure 2.6**, the release from the downstream glass logs is delayed significantly, the effect of ^{235}U decay becomes significant after 100 million years.

The maximum normalized mass for ^{235}U ranges between 0.0068 and 0.24 for the near-field rock porosity ranging between 0.01 and 0.5. This corresponds to the range between 220 mol and 7780 mol of ^{235}U.

The observations with **Figure 2.6** and **Figure 2.7** imply an important repository design option. Mainly due to their long half-lives, practically no effective confinement for uranium isotopes has been considered to be possible. However, from **Figure 2.6**, possibility of effective uranium confinement in the repository can be pointed out. If waste canisters are placed in such a way that they are lined up along the same water stream, the mechanism shown here makes the release of uranium from the repository to the far field considerably smaller. Furthermore, if we apply some engineering measures to decrease the near-field rock porosity to 0.01, from **Figure 2.7**, only 0.1% of uranium can be released before 100 million years. One of the possible measures is to use the bentonite buffer in the engineered-barrier region. Bentonite expands by water uptake and fills fractures in the near-field rock [11].

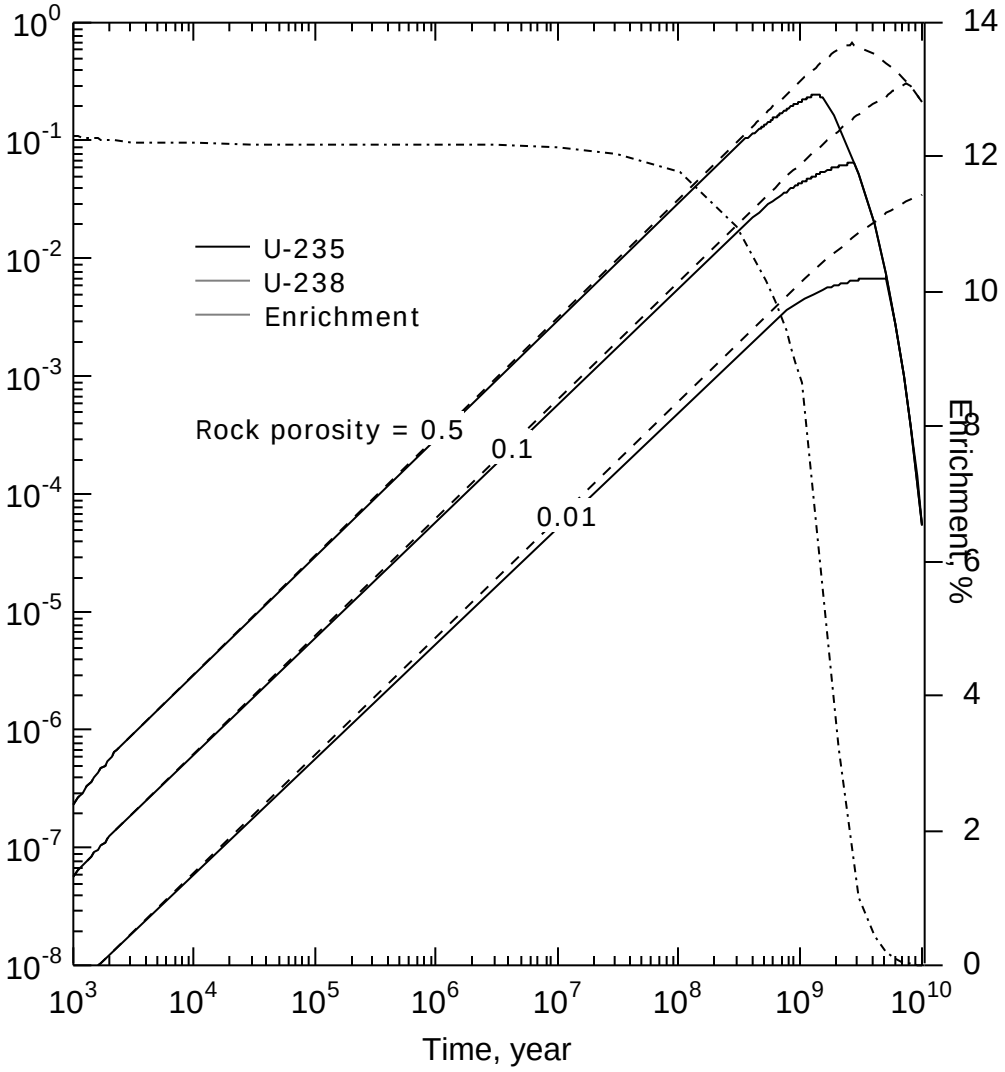

Figure 2.7 Effect of the near-fieldrock porosity on mass, $\overline{M}_k$, of uranium isotope *k*, existing in the far field.

2.7 Summary

We have found that

- It is unlikely that ^{239}Pu initially contained by 40,000 canisters in the repository with dimensions of 2 km _ 2 km can accumulate to a significant amount. The calculation result shows that at most less than one-billionth of the total initial mass of ^{239}Pu in 40,000 canisters can exist in the far field. Although calculation results have not been shown for other actinide species, such as Am and Np, same observations apply for such species due to their similar geochemical properties (low solubilities and relatively large sorption distribution coefficients with the host rock) and relatively short half-lives.
- The aforementioned observation allows us to simplify the transport model to a great extent. Uranium isotopes can be treated as single radionuclides without precursors. The masses of those precursors can be lumped to those of the uranium isotopes.
- With the effect of multiple canisters interfering each other taken into account, uranium release from the repository is decreased because the release from the downstream canisters is decreased significantly.
- Due to its shorter half-life, the interference effect is more significant for ^{235}U than for ^{238}U. ^{235}U decays within the glass logs more than ^{238}U. Thus, the enrichment of uranium existing in the far field starts to decrease with time after 100 million years.
- The maximum normalized mass of ^{235}U that exists in the far field ranges between 0.0068 mol and 0.24 mol for the rock porosity in the near field ranging between 0.01 and 0.5.
- The possibility of effective uranium confinement in the repository has been pointed out. If waste canisters are placed in such a way that they are lined up along the same water stream, the mechanism shown here makes the release of uranium from the repository to the far field considerably smaller. Furthermore, if we apply some engineering measures to decrease the rock porosity in the near field to 0.01, only 0.1% of uranium can be released before 100 million years. One of the possible measures is to use the bentonite buffer in the engineered-barrier region. Bentonite expands by water uptake and fills fractures in the near-field rock.

3. UNCERTAINTIES FOR TOTAL URANIUM MASS IN FAR FIELD

3.1 Introduction

The purpose of this chapter is to obtain the probability distribution function for the mass, $\overline{M}_{235}(t)$, of ^{235}U existing in the far field. Hereafter we omit the subscript 235.

In the previous chapter, we have observed the mechanisms that govern the mass transport in the repository. The major finding is that uranium is the principal fissile radionuclide that will be released into the far field. The total mass of ^{235}U in the far field has been selected as the performance measure of the repository criticality safety. Like other safety assessment, we consider the uncertainty associated with the performance measure in this chapter. At the end of this chapter, the performance measure will be expressed with its uncertainty bounds. This result will be compared in Chapter 4 with the safety criterion, which is, in the present case, the minimum critical mass of ^{235}U in a spherical accumulation.

The variation in the mass, $\overline{M}(t)$, occurs due to uncertainties associated with the parameters incorporated in the model described in the previous chapter. For example, the solubility of uranium has a wide range (10^{-5} ~ 10^{-7} mol/m^3) of uncertainty as indicated in the previous study [1]. The uncertainty of one parameter can be the result of uncertainties of other fundamental parameters. The uranium solubility is dependent on pH, the redox-potential, other solute species in the groundwater, the temperature, the rock type, and so on. Such fundamental parameters have uncertainties because they will change with time with an evolving geological environment and/or because they vary spatially due to heterogeneity of geologic formations. With quantitative geochemical simulation models [12], the uranium solubility can be estimated, based on those fundamental parameters. Therefore, if the repository site is determined, and the uncertainties of such fundamental parameters in a particular geological and geochemical environment are known, then the uncertainty with the uranium solubility can be better quantified.

In the current circumstances, where no repository site has been announced, we focus on generic behavior of the repository system assumed. Rather than determining a distribution function for a certain parameter based on distributions of its fundamental parameters, we determine a distribution function by collecting measurements of that parameter, available in literatures. If the number of data is not sufficient in supporting one distribution over another, we try normal, log-normal, uniform, and log-uniform probability distributions to observe the effect of the input-parameter distribution on the probability distribution of $\overline{M}(t)$. For geochemical parameters such as the solubility and the sorption distribution coefficients of uranium, a *log-normal* probability distribution function representing the data. For geometrical parameters such as porosities of the near-field rock and the buffer, the variation ranges can be specified more narrowly. In such a case, a normal distribution or a uniform distribution applies.

Based on the assumed probability distribution functions, parameter values are sampled. For each set of sampled parameter values, or realization, the computer code, developed in the previous chapter, is executed until the time step when the maximum for the mass, $\overline{M}(t)$, of ^{235}U is obtained. After many realizations, we obtain a frequency distribution for the maximum of $\overline{M}(t)$. Each frequency value is normalized by the total number of realizations.

3.2 Latin Hypercube Sampling

The conventional Monte Carlo method randomly selects values within the set of above mentioned parameters, based on the input probability density distribution function. Values selected have a higher tendency to concentrate around the mean within the standard deviation bounded by the limits. Due to the random method of selection, a large number of sampling must be repeated to ensure a good representation of the distribution function covering the entire range. The consequence is the need for high computing power and long simulation time.

Latin Hypercube Sampling (LHS) is another approach to repeated statistical sampling. LHS selects values for each input parameter in a structured manner. LHS was developed by McKay, Conover and Beckman [5] in 1975. LHS has been applied to many computer models since its development. Results and descriptions of its application to sensitivity analysis techniques [6, 7] have been scrutinized and investigated by many researchers. The computer code utilized in this study was developed by Iman and Shortencarier [8] in 1984.

From the cumulative density function (CDF) curve of an input parameter, the sections representing less than 0.001 probability at the extreme ends of the CDF distribution curve are neglected. The upper boundary (H) of the CDF is 0.999 and the lower end (L) is 0.001. The approximation eliminates the nuisance of incorporating infinity into the sampling. The mean and standard deviation of the distribution are defined as

$$\text{Mean} = \frac{H+L}{2}, \quad \text{Standard deviation} = \frac{H-L}{6.18}. \tag{16}$$

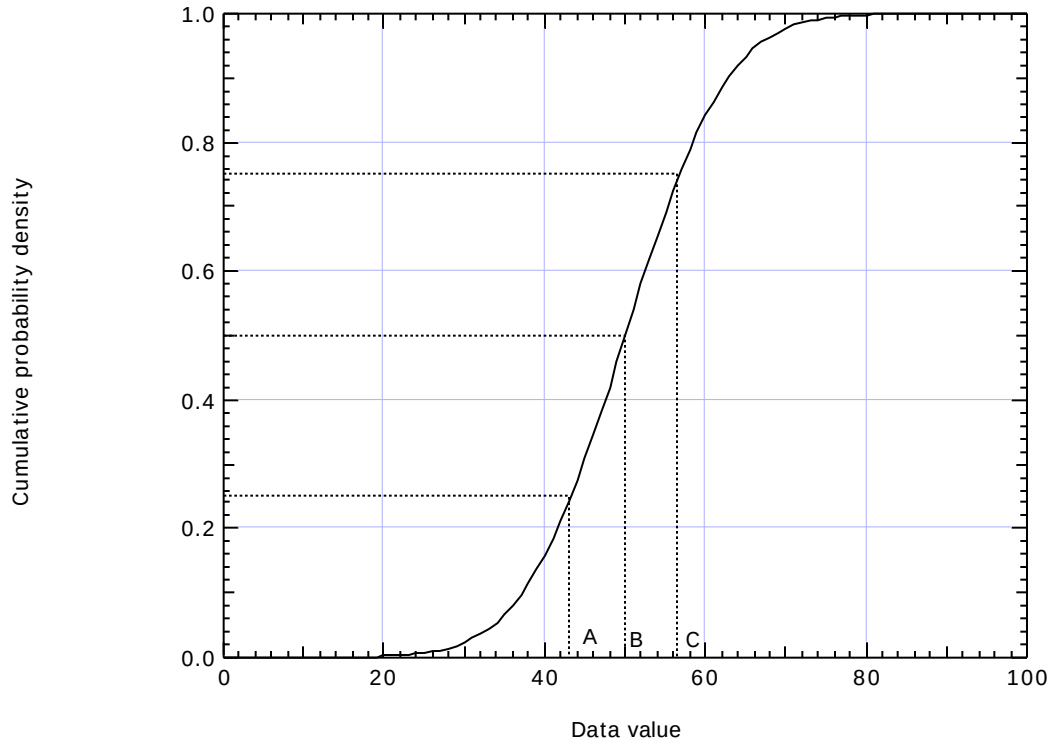

Figure 3.1 Cumulative probability density function for a normal distribution function sectioned into four equal bins with 0.1% truncation at the high and low ends.

The remaining 0.998 part of the CDF is divided into non-overlapping intervals on the basis of equal probability. For example, 4 non-overlapping intervals are devised within the 0.998 fraction. Each interval represents 0.998/4 = 0.249 or approximately 25% of the data value set for all practical purposes.

As shown in **Figure 3.1**, each section such as AB, represents approximately 25% of the probability curve. On the vertical cumulative probability density function axis, the intersections occur at 25%, 50% and 75%. They correspond to points A, B and C on the horizontal axis that represent the data values. By differentiating the CDF with respect to the data value variable, the probability density distribution function obtained is shown in **Figure 3.2**.

One value is selected from equally probable intervals with respect to the probability density within the interval. For example, with four intervals, each value signifies a 25% probability. The complete set of all four values composes a spectrum matching the profile of the chosen distribution function.

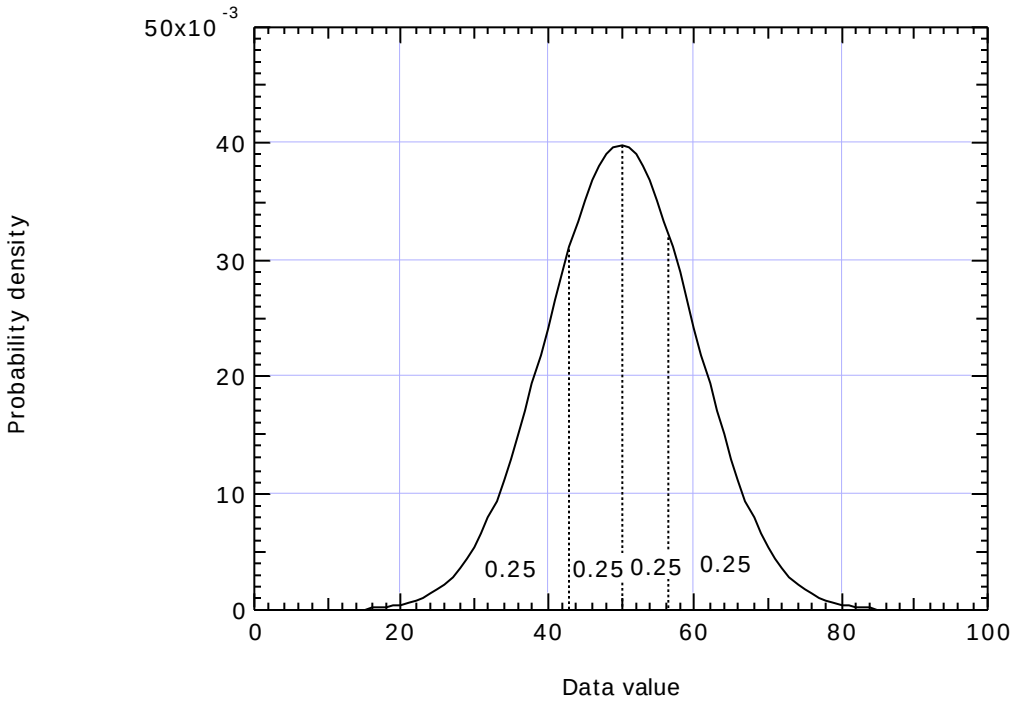

Figure 3.2 Density distribution function of a normally distributed function sectioned into four equal bins of approximately 25% each.

For each input parameter, a set of values is selected to represent the probability density distribution function. Each number is selected with equal probability across the spectrum. The complete set of selected values in turn represent the probability density distribution function in its entirety. The advantage of LHS over Monte Carlo is the reduced number of sampling for equally significant statistics. Values generated via Monte Carlo may represent the probability density distribution function only when a large number of values are sampled. With a smaller number of samples, Monte Carlo values are more likely to be biased by the high probability regions, such as the mean value and values within one standard deviation. The outer regions, where the probability is low and conservative values originate from, may not be adequately

represented. On the other hand, using LHS, the spectrum is represented regardless of the number of sampling since each value is selected from a region of equal probability to the others

Concurrently, a set of independent and representative input values is sampled for each parameter with the same number of intervals in the model evaluation. The values from each parameter are grouped into observations for simulation runs. The pairing of the input parameters is done in a random manner. LHS composes a matrix of the number of intervals by the number of input parameters with random combinations of all the input variables. Within each parameter, the values fully represent the specified probability density distribution function. Within each observation, all parameters are sampled with their respective functions.

In this study, cumulative density distribution functions for input parameters with variations have 100 divisions with equal probability.

3.3 Fixed Parameters

Several input parameters are fixed to single values throughout the entire analysis. The fixed parameters are denoted with the label "F" in the third column in **Table 2.3**. There are assumed to be 200 waste canisters in a row separated by a distance of 10 meters. The beginning of the modeling time is set at the start of radionuclide release from the glass log.

3.4 Parameters with Uncertainties

The ranges of variable inputs are summarized in **Table 3.1**.

Table 3.1 Ranges of Variable Parameter.

Parameter	Lower Bound	Upper Bound	Units
Water Velocity	0.1	10	m/yr
Near-Field Rock Porosity	0.001	0.5	
Buffer Porosity	0.23	0.43	
Buffer Diffusion Coefficient	0.001	0.1	m^2/yr
Sorption Distribution Coefficient in Rock	See **Figure 3.3**		m^3/kg
Sorption Distribution Coefficient in Buffer	0.1	100	m^3/kg
Uranium Solubility	See **Figure 3.4**		mol/m^3

3.4.1 Water velocity in the Near-Field Rock

In some cases, the velocity is fixed at 1.0 m/yr. The range of water velocity of 0.1 to 10 m/yr is used with an associated distribution function in other cases.

3.4.2 Porosity of the Near-Field Rock

The near-field rock porosity significantly affects the advective transport of radionuclides. The greater the near-field rock porosity is, the more radionuclides can be transported via groundwater flow downstream and exist in the far field. The capacity factor (see eq. (5)) in the near-field rock also depends on the rock porosity. The near-field rock porosity is assumed to range between 0.001 and 0.5 [2]. This range will be changed later to observe the effect of the near-field rock porosity on the mass, $\overline{M}(t)$, in the far field.

3.4.3 Porosity of the Bentonite Buffer

Porosity has a determining effect on the amount of radionuclide diffusing through the bentonite buffer. The retardation factor (see eq. (12)) in the buffer region also depends on the porosity of bentonite. A high porosity in the buffer results in a large amount of available radionuclide transported to the near-field rock. With an assumed value of 0.33 [2] as the arithmetic mean value, a uniform probability distribution for the buffer porosity ranging between 0.23 and 0.43 is assumed.

3.4.4 Diffusion Coefficient of Uranium in Buffer

The variation of the diffusion coefficient in bentonite occurs probably due to variation in tortuosity of the pore spaces in the bentonite region. A range of 1.0×10^{-3} to 1.0×10^{-1} m^2/yr is imposed on the parameter, based on [2, 13, 14].

3.4.5 Sorption Distribution Coefficient of Uranium in the Near-Field Rock

Since advection significantly affects the mass in the far field, so does the sorption distribution coefficient in the near-field rock. Thanks to the extensive collection of data by the Sorption DataBase [15], sufficient data pertaining to the study are extracted from the database. Only data pertaining to granite are considered and plotted in **Figure 3.3**. The circular dots represent the data collected via previous research and the solid line displays the log-normal distribution function with the mean and standard deviation taken from the actual data.

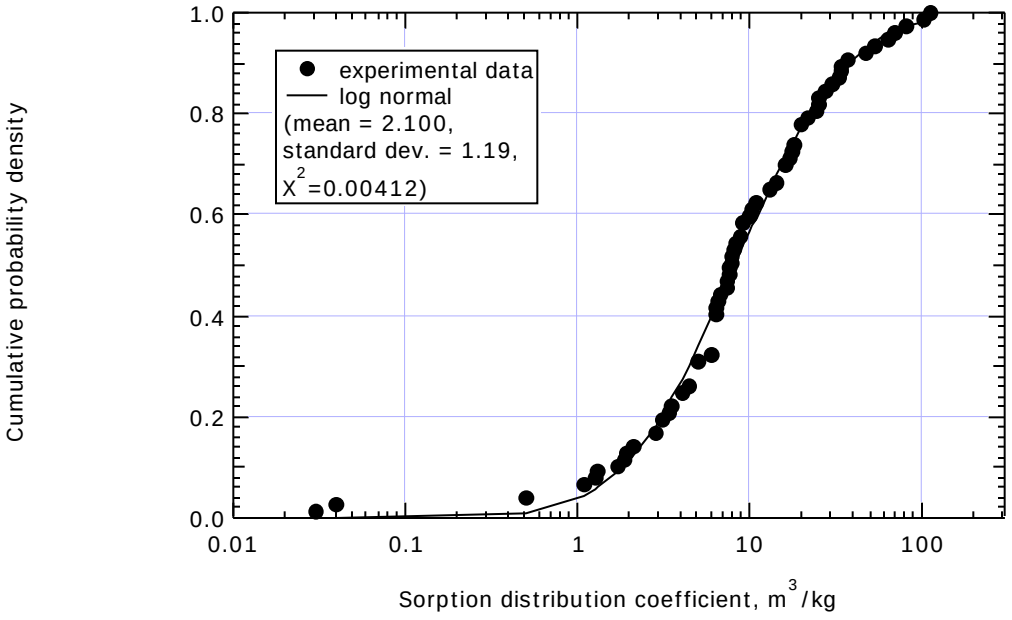

Figure 3.3 Cumulative probability density Function for sorption distribution coefficient of uranium

Data found in the database span several orders of magnitude. With the data at hand, a log-normal density distribution comes closest to the real data points. The best fitting log-normal distribution has a mean of 2.1 with a 1.19 standard deviation. The goodness of fit is justified by the Pearson's Chi-Square Statistics shown in (17),

$$X^2 = \sum_{i=1}^{n} \frac{(O_i - E_i)^2}{E_i} . \quad (17)$$

O_i denotes the i-th observation of real data points and n is the number of obtainable experimental data points. E_i indicates the corresponding expected value at the i-th occurrence. X^2 is the sum of the squares of all difference between observed and expected value divided by the expected value.

The smaller the X^2 is, the better the fit. Based on the limited data, the best fitting curve is a lognormal distribution function with a X^2 of 0.00412. The X^2 of a log-uniform fit is 2.07 while the mean and standard deviation are 0.25. Because the log-normal distribution has a much smaller X^2 value, the rock sorption distribution coefficient has been fitted by a log-normal distribution.

3.4.6 Sorption Distribution Coefficient of Uranium in Buffer

This parameter has a range between 0.1 m^3/kg and 100 m^3/kg taken in the previous study [1]. Just as for the sorption distribution coefficient in the near-field rock, a log-normal probability distribution function is assumed for the sorption distribution coefficient in the buffer.

3.4.7 Uranium Solubility

Data found corresponding to various rock types are utilized for determination of the distribution function for the uranium solubility. With the available data [16–19] on hand, data are compiled and plotted in **Figure 3.4**.

The mean of the best fitting curve is -19.95 with a standard deviation of 1.05. The X^2 value is 0.4068. Based on the Pearson's Chi-Square method, a log-normal distribution function fits the experimental data points much better than the log-uniform and normal distribution functions.

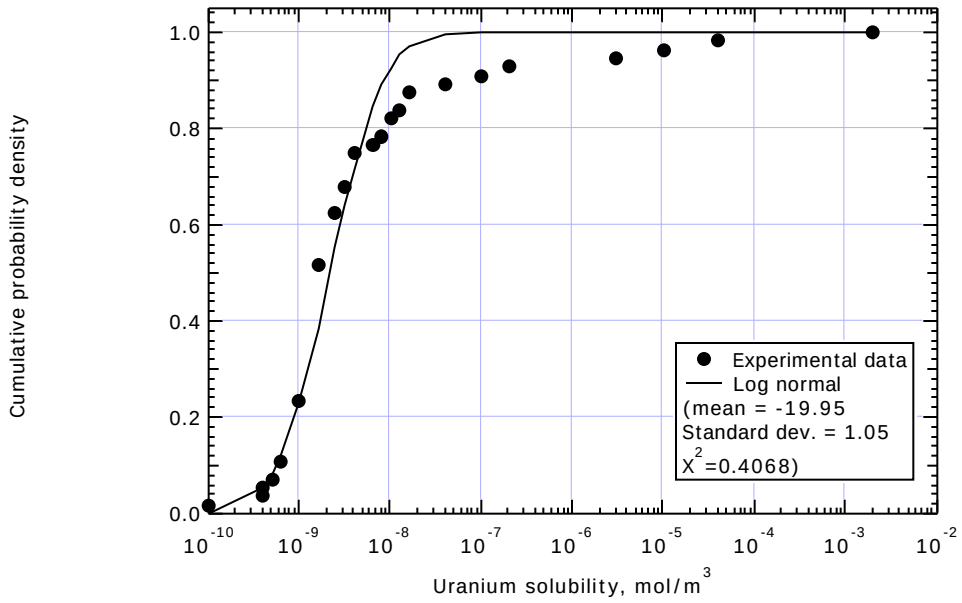

Figure 3.4 Cumulative probability density function for solubility of uranium

3.5 Effect of Number of Realizations

Table 3.2 shows the assumed input parameter distributions for observation of the effect of the number of realizations. The input distributions are log-normal for the major variables. Buffer and the near-field rock porosities have uniform distributions. Water velocity is fixed at 1.0 m/yr.

From **Figure 3.5**, it is obvious that 4,000 realizations produce a smoother curve than 500 realizations. Calculations for 4000 realizations is time-consuming. The attention turns to either 1000 or 2000 data points per case. **Figure 3.6** portrays the density distribution functions of 1000 and 2000 data points. The 2000-realization spectrum has a smoother curve than that of 1000 realizations.

Table 3.2 Assumed Input Parameter Distributions for Observation of the Effect of Realization Number

Parameter	Distribution
Water Velocity	Fixed (1.0 m/yr)
Near-Field Rock Porosity	Uniform
Buffer Porosity	Uniform
Buffer Diffusion Coefficient	Log-normal
Sorption Distribution Coefficient in Rock	Log-normal
Sorption Distribution Coefficient in Buffer	Log-normal
Uranium Solubility	Log-normal

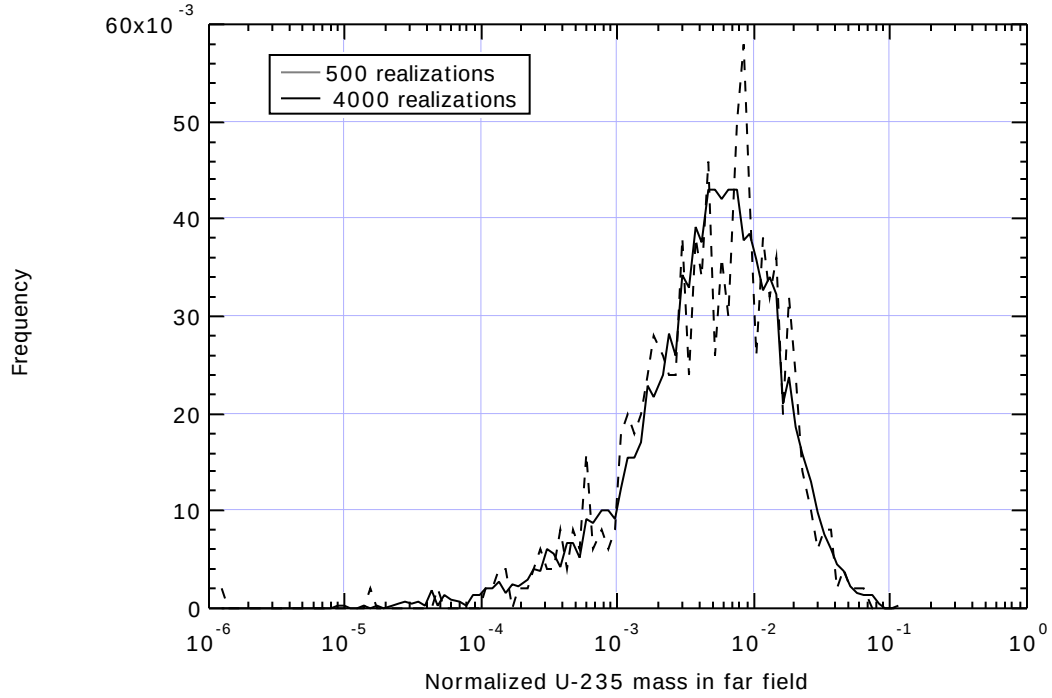

Figure 3.5 Difference in frequency distributions obtained by 500 realizations and 4,000 realizations.

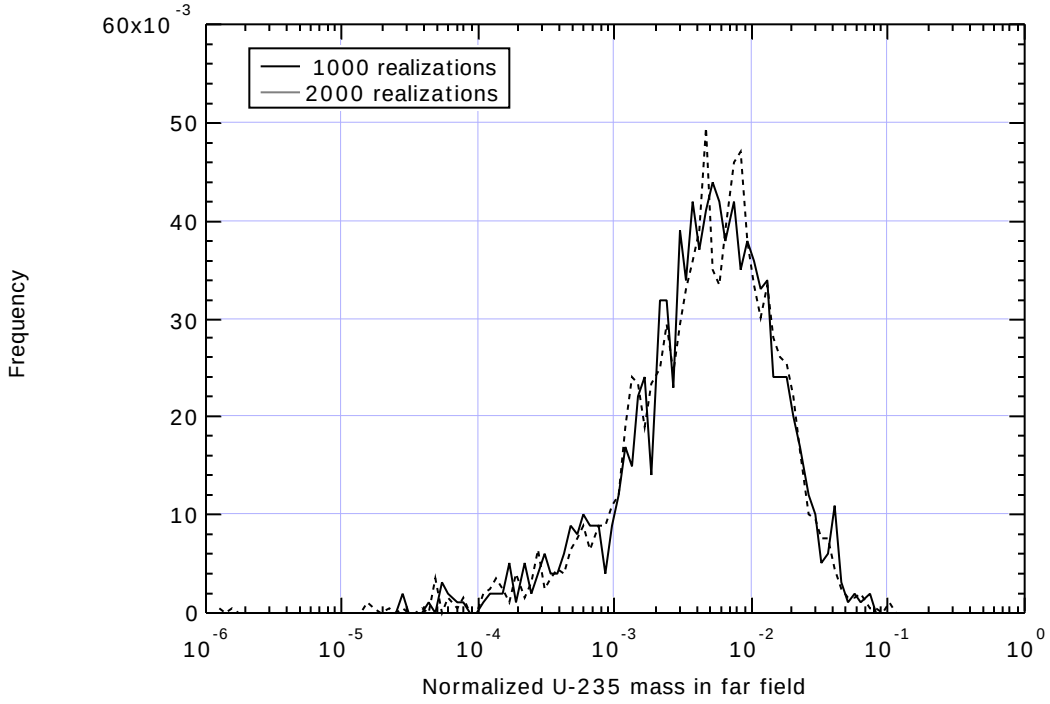

Figure 3.6 Difference in frequency distributions obtained by 1,000 realizations and 2,000 realizations.

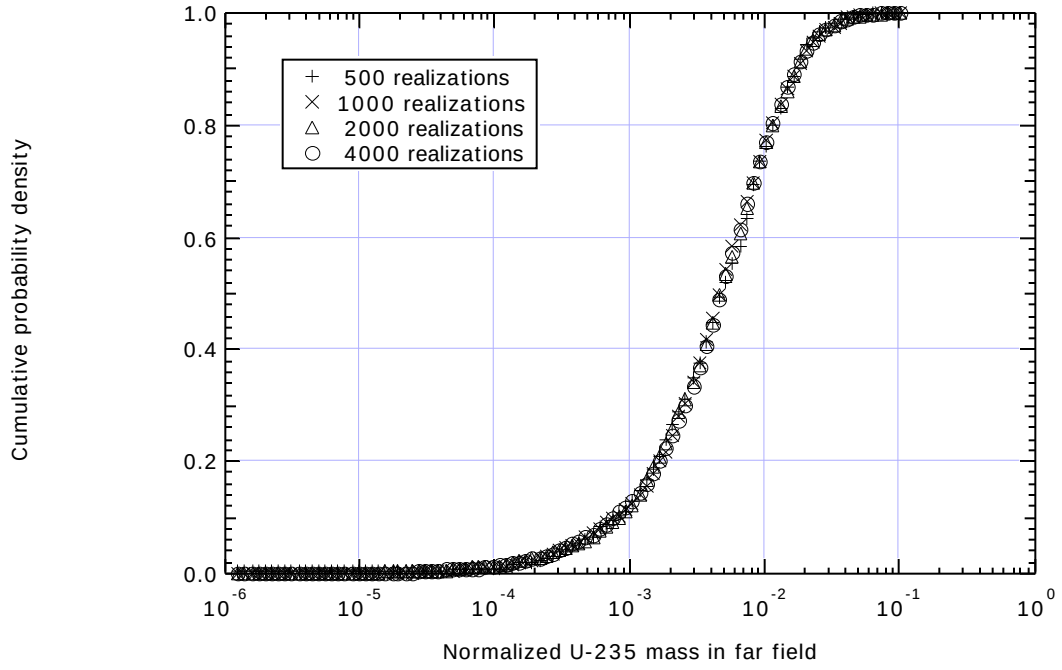

Figure 3.7 Cumulative probability density functions of normalized ^{235}U mass in the far field for four different total realizations.

Figure 3.7 depicts the cumulative probability density for four different numbers of realizations. In spite of fluctuations observed in **Figure 3.5** and **Figure 3.6**, the curves for the cumulative probability density overlap with each other, which implies that 4,000 realizations are not necessary to obtain fundamental statistical characteristics. Hereafter, 2,000 realizations are calculated per case.

3.6 Effect of Distribution Functions

Combinations of the distribution functions to be investigated in this section are summarized in **Table 3.3**. Water velocity has a normal distribution, with the median of 2.5 m/yr. The ranges and fixed values of the input parameters are the same as those in **Table 3.1** and **Table 2.3**.

For cases (1), (2), and (3), the distribution functions for the diffusion coefficient, the sorption distribution coefficients both in rock and buffer, and the solubility are the same within each case.

For case (4), log-normal distributions are assumed for the sorption distribution coefficients whereas log-uniform distributions are assumed for the diffusion coefficient and the solubility. The distribution function for the near-field rock porosity is assumed to be normal. This makes values around the mean (0.25) occur more frequently.

Table 3.3 Summary of Input Parameter Distributions and Statistics of the Resultant Distribution.

Parameter	**Case (1)**	**Case (2)**	**Case (3)**	**Case (4)**
Water Velocity	N	N	N	N
Near-field rock Porosity	U	U	U	**N**
Buffer Porosity	U	U	U	U
Buffer Diffusion Coefficient	**LN**	**LU**	**N**	**LU**
Sorption Distribution Coefficient in Rock				**LN**
Sorption Distribution Coefficient in Buffer				**LN**
Uranium Solubility				**LU**
Statistics for normalized mass of U-235 in the far field				
5-Percentile	5.90E-06	5.20E-08	2.88E-06	6.26E-06
Median	7.22E-04	2.40E-04	4.85E-05	9.70E-04
95-Percentile	2.53E-02	6.05E-02	2.67E-04	5.33E-02
99-Percentile	6.09E-02	1.67E-01	4.23E-04	1.84E-01

N: Normal; U: Uniform; LN: Log-Normal; LU: Log-Uniform.

Figure 3.8 illustrates the effects of the input parameter distribution functions. The bottom half of **Table 3.3** shows the numerical values of the statistically interesting points.

In the top figure of **Figure 3.8**, the locations of the maximum masses that can be read from the three curves for ^{235}U in **Figure 2.7** are pointed out along the horizontal axis. It is observed that the three cases considered in the previous chapter give relatively large values of the maximum mass of ^{235}U in the far field among possible realizations. Especially, the case with

the porosity of 0.5 in the near field rock seems very unlikely to happen for any combinations of probability density distribution functions for parameters.

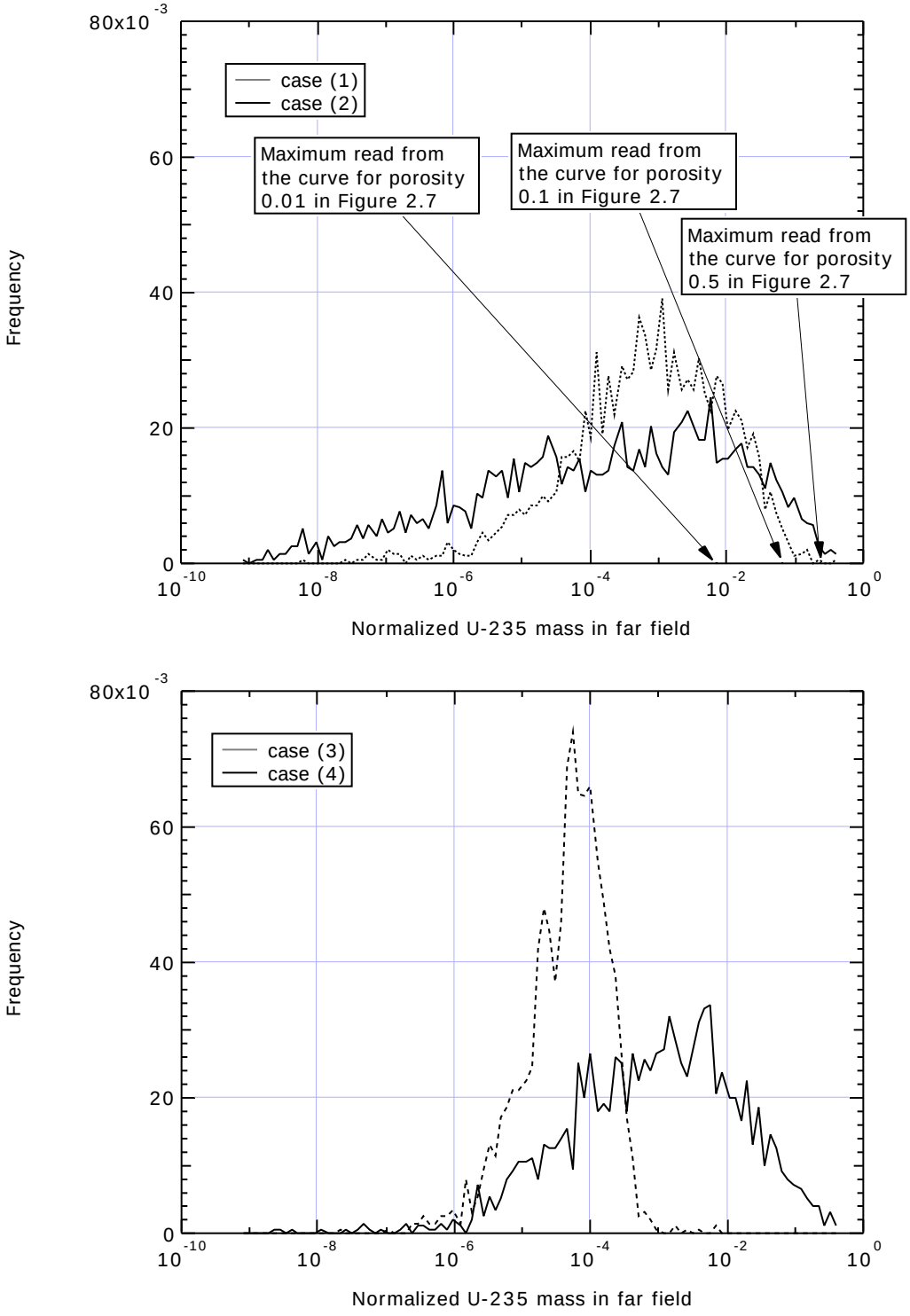

Figure 3.8 Frequency curves for the normalized mass of ^{235}U in the far field with combinations of distribution functions shown in Table 3.4

The frequency curve resulting from the normal distribution (case (3)) resembles a normal distribution; the resultant distribution based on normally-distributed input parameters is much narrower than other resultant distributions, and so the uncertainty is the smallest in this case than other three cases compared here. In **Table 3.3,** it is observed that the statistically interesting points of log-normal and log-uniform functions are closer together than they are to results from normally distributed input parameters. The input values chosen for the simulations spread several orders of magnitude on the logarithmic scale. With a larger variability of input values, the output spans across several orders of magnitude more than with normally distributed input parameter values.

However, it is appropriate to assign a log-normal distribution to such parameters as the solubility and the sorption distribution coefficients because they actually have a wide range of variations as shown in **Figure 3.3** and **Figure 3.4**. Case (3) result implies that, for a more reliable safety assessment for a geologic repository, we should obtain a distribution like case (3), for which the uncertainties associated with each parameter should be characterized as a normal distribution, rather than a widely-ranging log-normal or log-uniform distribution.

The distribution resulting from the log-uniform distributions (case (2)) displays a spectrum with a lowest density at the mean value comparing to the log-normal distribution case (case (1)). The high percentile values from the log-uniform distribution are higher than those from the log-normal distribution.

With the heterogeneous combination of distribution functions (case (4)), the curve has a higher mean frequency than the case (2) curve but lower than the case (1) curve. At the high percentile region, the heterogeneous curve coincides with the log-uniform curve (case (1)). At the low percentile region, the log-normal curve (case (2)) matches closer to the heterogeneous case.

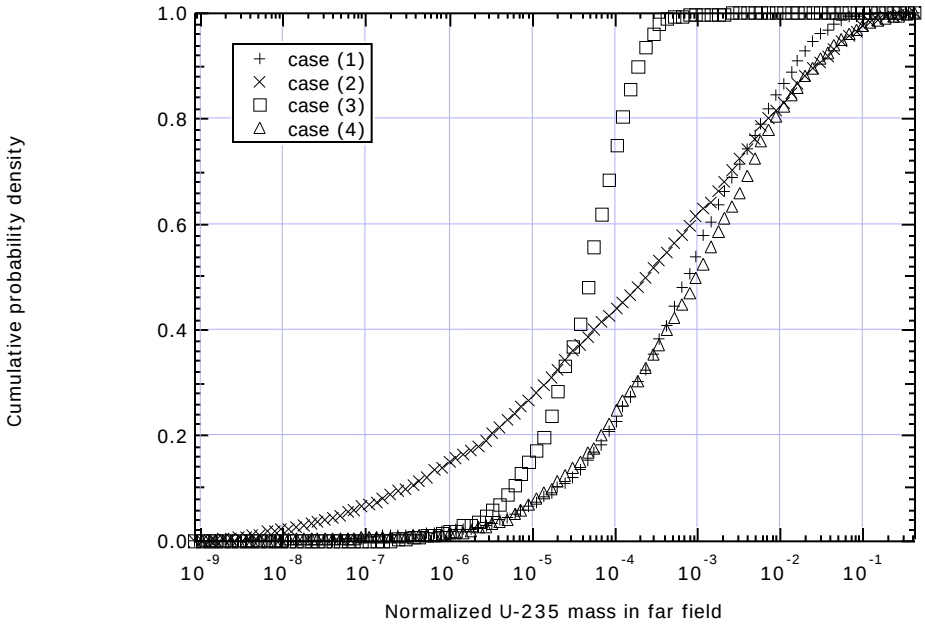

Figure 3.9 Cumulative probability density functions for the normalized mass of uranium in the far field for four different combinations of input probability density functions.

In **Figure 3.9**, the cumulative probability distributions are plotted for these four cases. Among the four combinations, case (3) shows quite a different distribution from other cases. The distribution for case (4) is similar to that for case (1) for the low-mass region, whereas the distribution for case (4) coincides with that for case (2) for the large-mass region.

3.7 Effect of Near-Field Rock Porosity

Due to their long half-lives, decay loss during the diffusion in the buffer is negligible for uranium isotopes. Major reduction of uranium mass occurs during the advective transport in the near-field rock and the host rock in the far field. In this section, we artificially vary the ranges of the effect of the near-field rock porosity, and observe its effects.

3.7.1 Cases Considered

In case (5) of **Table 3.4**, a low-range host rock porosity (0 ~ 0.02) is set, which is compared to the normal range (0.001 ~ 0.5) for the near-field rock porosity (case (6a)). The ranges and distribution functions of the other major input parameters for cases (5) and (6a) remain the same as those of case (1). Water velocity is fixed at 1.0 m/yr. Porosities of the near-field rock and the buffer are assumed to have uniform distribution functions.

Although a repository should be built in geologic formations with a low porosity, other considerations may make this criterion difficult comprised with. For example, from a viewpoint of HLW canister transportation, a seashore area might be selected for the repository site. A coarser host rock formation may exist at the seashore. Thus, simulations of higher host rock porosity are conducted. The near-field rock porosity is increased from a range of 0.001 to 0.5 to a higher range 0.2 to 0.6, with a normal distribution (cases (6b) and (7)). The mean value of the near-field rock porosity of case (7) is 0.4 comparing to 0.25 in case (6b). Note that the density distribution function is normal instead of uniform. The near-field rock porosity values close to the mean value occur more frequently. Water velocity ranges from 0.1 m/yr to 10 m/yr with a normal distribution function. This setup gives a mean velocity of 2.5 m/yr, which is greater than 1.0 m/yr in cases (5) and (6a). The rest of the major input parameters have log-normal distribution functions and unaltered ranges.

3.7.2 Results

It is observed in **Figure 3.10** that a greater near-field rock porosity leads to more mass in the far field. While both curves display similar density distribution functions, there is a distinct difference in the magnitude. The standard deviation of both curves appears to be the same. This can be explained by the identical ranges and density distribution functions implemented for all input parameters during the simulation, with the exception of the near-field rock porosity range.

Figure 3.12 shows the cumulative distributions for cases (5) and (6a). Both curves are similar to each other. The high-porosity case (6a) gives two orders of magnitude greater mass in the far field.

Table 3.4 shows that as the mean of the near-field rock porosity is increased from 0.01 (case (5)) to 0.25 (case (6a)), the mean value of the mass for the high porosity case (6a) is roughly a factor of 24 greater than that for the low porosity case (5). At the 5-percentile mark, high porosity group is approximately 24 times higher. Similar trend is observed at the high percentile regions also.

Figure 3.11 shows again that with a greater near-field rock porosity more mass of uranium exists in the far field. **Table 3.4** shows that the mean value of case (7) is approximately

1.5 times as high as that of case (6b). The difference in the cumulative distributions between case (6b) and case (7) is, however, not so prominent as that between case (5) and (6a), as is also confirmed by **Figure 3.12**. That is because the porosity ranges do not overlap with each other significantly between cases (5) and (6a) whereas the major portion of the porosity ranges overlap with each other between cases (6b) and (7).

The cumulative probability density for case (6a) is significantly different from that for case (6b), although the porosity range is identical in these two cases. In case (6a), the near-field rock porosity has a uniform distribution while in case (6b) a normal distribution with the mean value of 0.25 is assumed for the near-field rock porosity. In addition, groundwater velocity is a constant of 1.0 m/yr in case (6a) while in case (6b), it possesses a normal distribution function with a range of 0.1 to 10 m/yr at a mean of 5.0 m/yr, five times higher than 1.0 m/yr. This comparison shows that the effect of water velocity also has a strong influence over the mass in the far field. To make the large mass existence in the far field less likely, it must be assured that the near-field rock porosity and the water velocity in the repository are sufficiently small.

Table 3.4 Distribution and Ranges for the Study of Host Rock Porosity Range and Statistics of the Resultant Distributions

Parameter	**Case (5)**	**Case (6a)**	**Case (6b)**	**Case (7)**
Water Velocity	Fixed (1.0 m/yr)		Normal (0.1 ~ 10 m/yr) (Same as cases (1) ~ (4))	
Near-Field Rock Porosity	Uniform 0 ~ 0.02	Uniform 0.001~ 0.5 (same as cases (1) ~ (3))	Normal 0.001 ~ 0.5 (same as case (4))	Normal 0.2 ~ 0.6
Buffer Porosity	Uniform (same as cases (1) ~ (4))			
Buffer Diffusion Coefficient	Log-normal (same as case (1))			
Rock Sorption Coefficient				
Buffer Sorption Coefficient				
Uranium Solubility				
Statistics for normalized mass of U-235 in the far field				
5-Percentile	1.54E-05	3.91E-04	1.12E-05	2.12E-05
Median	1.90E-04	4.68E-03	9.53E-04	1.98E-03
95-Percentile	1.04E-03	2.27E-02	2.69E-02	3.89E-02
99-Percentile	1.73E-03	4.04E-02	6.33E-02	9.23E-02

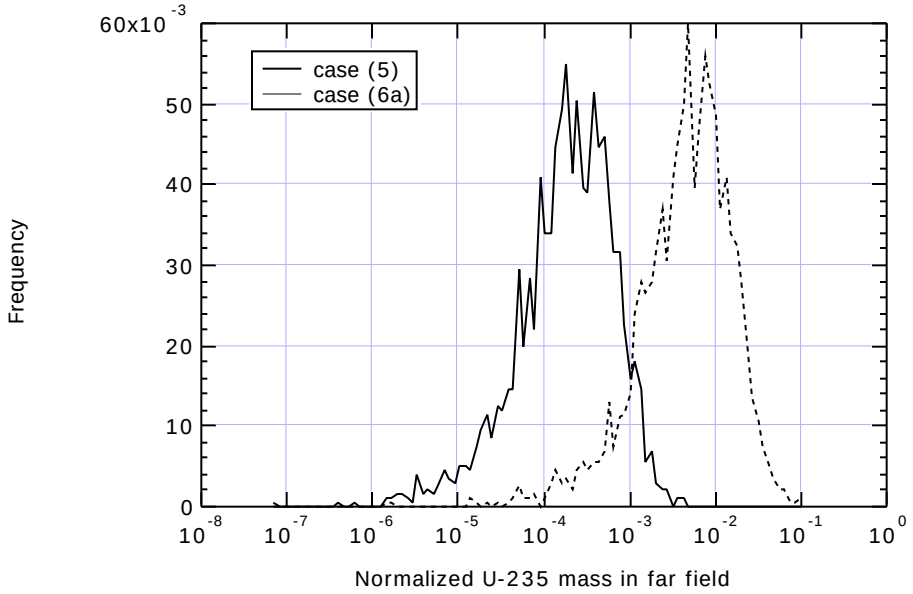

Figure 3.10 Frequency curves for the normalized ^{235}U mass in the far field with low (case (5)) and normal (case (6a)) near-field rock porosity ranges

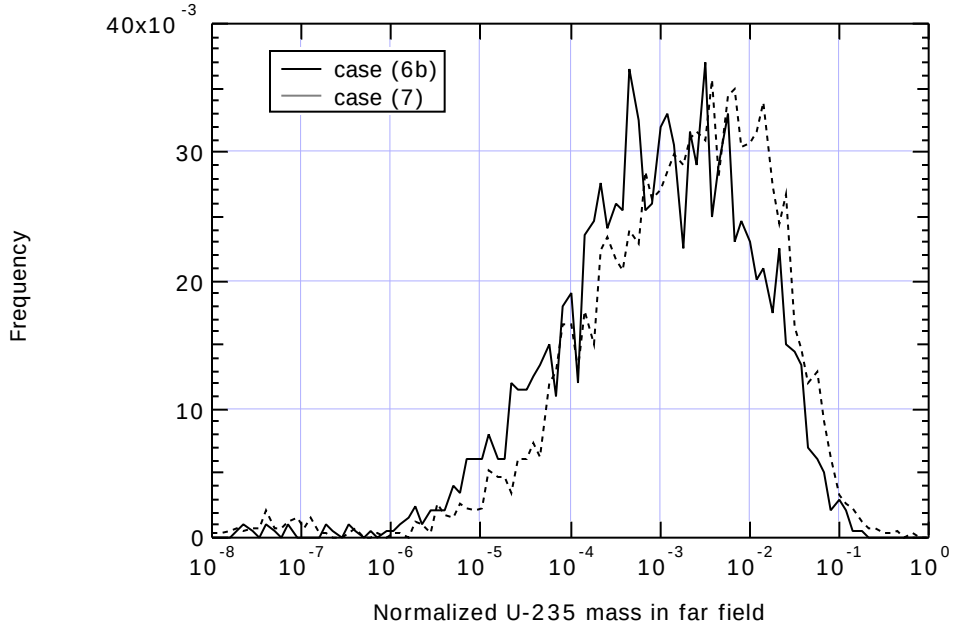

Figure 3.11 Frequency curves for the normalized ^{235}U mass in the far field with low (case (6b)) and normal (case (7)) near-field rock porosity ranges

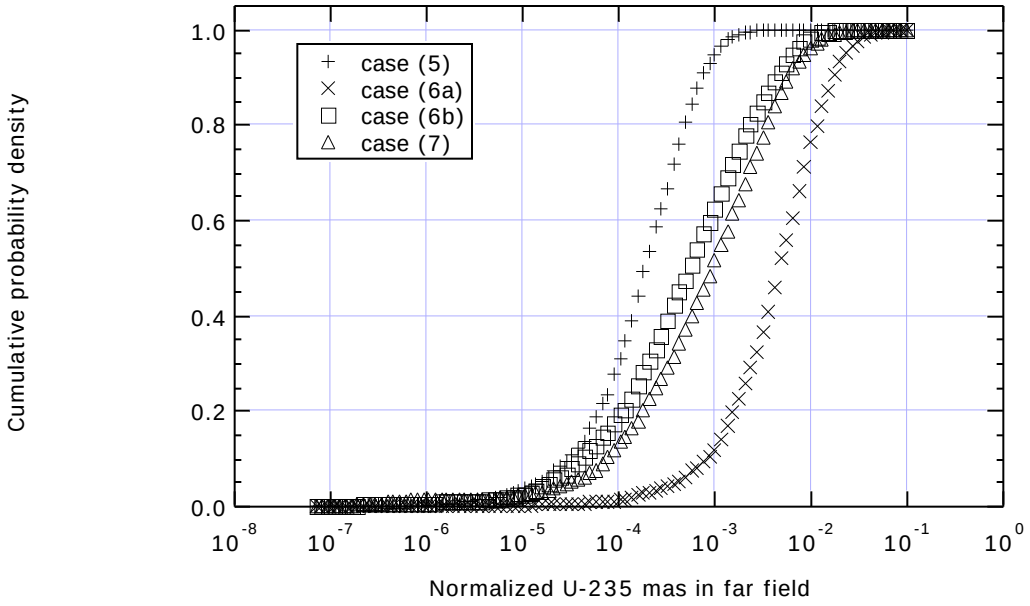

Figure 3.12 Cumulative probability density functions for the normalized mass of uranium in the far field for different rock porosity distributions.

3.8 Summary

We have found that

- 2,000 realizations are sufficiently many to obtain statistically significant results. For the cumulative probability density function, the difference between the 500 realizations and 4,000 realizations is negligible.
- With currently available data, a log-normal distribution is an appropriate representation for uncertainties associated with the sorption distribution coefficients, the uranium solubility, and the diffusion coefficient. With more data and the repository site determined, the uncertainties with these parameters should be represented by a normal distribution, which gives more reliable estimate of the mass in the far field.
- With the near field rock porosity ranging between 0 and 0.02 uniformly (case (5)), the maximum normalized mass of ^{235}U in the far field is found to be within the range between 1.54×10^{-5} and 1.04×10^{-3} with the median of 1.90×10^{-4}, with the 90% confidence.
- With the near field rock porosity ranging between 0.001 and 0.5 normally and the water velocity ranging between 0.1 and 10 m/yr normally (case (6b)), the maximum normalized mass of ^{235}U in the far field is found to be within the range between 1.12×10^{-5} and 2.69×10^{-2} with the median of 9.53×10^{-4}, with the 90% confidence.
- If the near field rock porosity range changes to between 0.2 and 0.6 (case (7)), the maximum normalized mass of ^{235}U in the far field increases by 50%.
- In any case, the maximum normalized mass of ^{235}U in the far field remains less than 0.05 with the 90% confidence. Because the total initial mass of ^{235}U in the repository

is 32,400 mol, the maximum mass of ^{235}U in the far field is less than 1,620 mol, or 380 kg of ^{235}U.

- From **Figure 2.7**, the maximum occurs at one billion years or later. If the time span for the safety assessment is arbitrarily set to be 100 million years, the total mass in the far field at that time is estimated approximately one order of magnitude smaller than the maximum. Thus, the total mass of ^{235}U in the far field at 100 million years is likely to be less than 40 kg.

4. DISCUSSION

In Chapter 2, a deterministic mathematical model has been established, with which the maximum mass of ^{235}U existing in the entire far field can be estimated. The maximum mass of ^{235}U existing in the entire far field has been chosen as the performance measure for the repository safety from the viewpoint of criticality safety. Based on the numerical evaluations with the model, it has been pointed out that, because the mass of ^{239}Pu is at any time negligibly small, ^{235}U is the only fissile material that will be available for a sufficiently long time. Three cases have been considered for different values of the porosity in the near field rock for estimating the mass of ^{235}U existing in the far field. The results in **Figure 2.7** show that if the parameters in the model has uncertainties like the porosity in the near field rock, the value of the mass of ^{235}U existing in the entire far field can have significant uncertainties.

Thus, for the judgement of the repository safety, a single number of the performance measure obtained by the deterministic analysis like the one shown in Chapter 2 should not be compared directly with the safety criterion. The performance measure to be compared with the safety criterion must accompany the uncertainty information.

In Chapter 3, only uncertainties arising from the model parameter distributions, i.e., data uncertainties, are taken into account. No considerations have been made for uncertainties arising from the differences in model assumptions. Such uncertainties, i.e., scenario uncertainties, should be discussed in more detail after the repository site is determined.

The data uncertainties have been considered in Chapter 3 by performing a Monte Carlo analysis with the model developed in Chapter 2. As a result of the statistical analysis, the performance measure can be expressed not just by a single value but by a range of possible values with a corresponding confidence level.

At the end of Chapter 3, the results of the statistical analysis have been summarized as follows. The maximum mass of ^{235}U existing in the entire far field is at any time less than 5% of the mass of ^{235}U and its precursors initially available in the repository with a 90% confidence. If the repository performance is considered in the time span of 100 million years, the largest mass of ^{235}U existing in the entire far field is approximately one order of magnitude smaller than the maximum mass. This result can be compared with an appropriate criterion for criticality safety of a geologic repository.

Currently, there is no specific criterion for criticality safety of a water-saturated repository regarding the scenario for accumulation of fissile material in the far field. To establish that, the mechanisms for the transport and accumulation of fissile material in the far field must be known. The intent of this report is the following. The maximum mass of ^{235}U existing in the far field is the theoretical upper bound of the mass of fissile ^{235}U available for accumulation in some regions of the far field. On the other hand, a mass of ^{235}U required for criticality is determined by the geometry of these regions and the constituent materials in the accumulation. In this study, minimum critical masses of 12%-enriched uranium in a spherical geometry surrounded by a 120-cm thick rock reflector, which were studied in the previous report [1], are used as the safety criterion. The results of the present work are to be compared with the minimum critical masses of that configuration obtained in [1].

In the previous report [1], with a porosity of 0.1, the minimum critical mass was found to be 60 kg of ^{235}U, with a core radius of 90 cm, as shown in **Table 4.1**. 7.0 kg of ^{235}U was found to be sufficient to form an under-moderated critical configuration with a core radius of 37 cm. In

over-moderated formation, criticality was not achievable with granite porosity of 0.1 while it could be reached at 35 kg in a 90-cm radius spherical formation with a porosity of 0.3. While critical systems made by homogeneous 12%-enriched uranium can not be autocatalytic beyond a small initial power excursion, due to over-moderation, critical systems made by heterogeneous deposition of 12%-enriched uranium in saturated medium can be autocatalytic, as the combined reactivity effect of uranium and rock temperature increase can be positive.

Table 4.1 Summary of Minimum Critical ^{235}U Masses [kg] / Core Radii [cm] for Homogeneous, Spherical, Reflected $U(12)O_2$ + Rock + H_2O Systems [1]

Medium / Porosity	Minimum critical mass [kg] /Core radius [cm]	
	Minimum under-moderated	Minimum over-moderated
Water	1.5 / 19	—
SiO_2 / 0.1	17 / 71	48 / 130
Granite / 0.1	60 / 90	infinite
Granite /0.3	7.0 / 37	35/90

From the results obtained in Chapter 3, the total mass of ^{235}U in the far field at 100 million years is likely to be less than 40 kg. To be over-moderated, almost all ^{235}U existing in the far field at 100 million years must accumulate at a single location within a radius of 90 cm in granite with a porosity of 0.3. Accumulation of all ^{235}U into a single location is unlikely to happen, if one considers that the transport of radionuclides in the groundwater must converge to the accumulation region and the favorable geochemical conditions must be kept.

This finding poses a concern over the validity of direct comparison between the two studies. The geometry and configuration of radionuclide accumulation are not implemented in the transport model in Chapter 2. The results obtained in minimum critical mass study in the previous report [1], on the other hand, are geometry dependent. A homogeneous spherical mixture of water, host rock and radionuclides is the basis of the study. In actuality, accumulation is not likely to form a spherical configuration with the specified radius and density.

The number (< 40 kg) obtained by the transport analysis is the *total* mass existing in the *entire* far field. Therefore, this is the theoretical maximum for the mass that can potentially accumulate. Furthermore, with the parameter uncertainties, the probability of exceeding this number is 10%. The ranges of parameter variations have been determined based on the available data for a wide variety of granitic rocks. Thus, the parameter uncertainties considered here cover typical granitic rocks, and the number obtained here by the transport analysis is generic for many granitic-rock repositories.

The minimum critical masses can also be different in a real situation from those obtained in [1]. However, in reality, the minimum critical mass will be even greater than those shown in **Table 4.1** because the uranium accumulation will be more likely to be heterogeneous.

With these considerations, the following conclusion is derived. It is highly unlikely that a sufficient mass of uranium for autocatalytic criticality accumulates in the far field, originating from borosilicate HLW glass logs in a water-saturated granitic rock formation. Although this conclusion is valid for a wide variety of granitic rocks, a site-specific study should be still recommended after a repository site is determined.

5. CONCLUSION

A model for radionuclide transport in the repository region has been established by taking into account the effect of multiple canister interference. With the model, the numerical evaluations have been performed for ^{239}Pu, ^{235}U, and ^{238}U. We have found that

- A negligibly small fraction of ^{239}Pu initially existing in 40,000 canisters can exist in the entire far field at any time.
- Uranium release from the repository is decreased and the time span for the release is increased because the release from the downstream canisters is decreased significantly.
- Due to its shorter half-life, the interference effect (shown in **Figure 2.1** is more significant for ^{235}U than for ^{238}U. ^{235}U decays within the glass logs more than ^{238}U. Thus, the mass fraction of ^{235}U over total uranium existing in the far field starts to decrease with time after 100 million years.
- The possibility of effective uranium confinement in the repository has been pointed out. If waste canisters are placed in such a way that they are lined up along the same water stream, the mechanism shown here makes the release of uranium from the repository to the far field considerably smaller. Furthermore, if we apply some engineering measures to decrease the near-field rock porosity to 0.01, only 0.1% of uranium can be released before 100 million years.
- With the assumed probability distribution functions for the model parameters, the maximum normalized mass of ^{235}U in the far field remains less than 0.05 with a 90% confidence. Because the total initial mass of ^{235}U in the repository is 32,400 mol, the maximum mass of ^{235}U in the far field is less than 1,620 mol, or 380 kg of ^{235}U.
- If the time span for the safety assessment is arbitrarily set to be 100 million years, the total mass in the far field at that time is estimated approximately one order of magnitude smaller than the maximum. Thus, the total mass of ^{235}U in the far field at 100 million years is likely to be less than 40 kg.
- Although these conclusions of this report are valid for a wide variety of granitic rocks, a site-specific study should be still recommended once a repository site is determined.

6. REFERENCES

[1] J. Ahn, S. Armel, J. Burch, P. L. Chambré, E. Greenspan, and D. A. Roberts, *Underground Autocatalytic Criticality from Fissile Materials Solidified in Borosilicate Glass*, UCBNE-4218, Department of Nuclear Engineering, University fo California, Berkeley, (1997).

[2] Power Reactor and Nuclear Fuel Development Corporation, *Technical Report on Research and Development for Geological Disposal of High-Level Radioactive Wastes*, PNC TN 1410 92-08 (1992).

[3] Svensk Karnbranslehantering Ab, SKB91: Final disposal of spent nuclear fuel. Importance of the bedrock for safety, SKB Technoical report 92-20 (1992).

[4] NAGRA, Kristallin-I: Safety Assessment Report, Tech. Rep. 93-22E, NAGRA, Wettingen, Switzerland (1994).

[5] M.D. McKay, W.J. Conover and R.J. Beckman, "A Comparison of Three Methods for Selecting Values of Input Variables in the Analysis of Output from a Computer Code", Technometrics, 21 (2), PP. 239-245

[6] R. L. Iman, J. C. Helton and J.E. Campbell, "An Approach to Sensitivity Analysis of Computer Models Part 1. Introduction, Input Variable Selection and Preliminary Variable Assessment", *Journal of Quality Technology*, **13**(3), 174-183

[7] R. L. Iman and J. C. Helton, "A Comparison of Uncertainty and Sensitivity Analysis Techniques for computer Models, Part 2. Ranking of Input Variables, response Surface Validation, Distribution effect and technique Synopsis", *Journal of Quality Technology*, **13**(4), 232-240

[8] R. L. Iman and M. J. Shortencarier, *A FORTRAN 77 Program and User's Guide for the Generation of Latin Hypercube and Random Samples for Use with Computer Models*, , SAND83-2365, NUREG/CR-3624, Sandia National Laboratories (1984)

[9] A. G. Croff, *A User's Manual for the ORIGEN 2 Computer Code*, ORNL/TM-7175, Oak Ridge national Laboratory (1980).

[10] J. Ahn, T. Ikeda, T. Ohe, T. Kanno, Y. Sakamoto, T. Chiba, M. Tsukamoto, S. Nakayama, S. Nagasaki, K. Banno, and T. Fujita, Quantitative Performance Allocation of Multi-Barrier System for High-Level Radioactive Waste Disposal, *Journal of Atomic Energy Society of Japan*, **37**(1), 59-77 (1995).

[11] J. Verbeke, J. Ahn, and P. L. Chambré, *Long-Term Behavior of Buffer Materials in Geologic Repositories for High-Level Wastes*, UCB-NE-4220, University of California, Berkeley, 1997.

[12] D. L. Parkhurst, et.al., PHREEQE: A Computer program for geochemical calculations, USGS/WRD WRI-81/018, U. S. Geological Survey (1980).

[13] K. Idemitsu, H. Furuya, Y. Tachi and Y. Inagaki, "Diffusion of Uranium in Compacted Bentonite in the Presence of Carbon Steel", Scientific Basis for Nuclear Waste Management, Vol. 333, pp. 939-946, 1994

[14] L. Romero, A. Andersson, L. Moreno and I. Neretnieks, "Radionuclide Release from the KBS-3 Repository - Sensitivity to the Variability of Materials and Other Properties", Scientific Basis for Nuclear Waste Management, Vol. 353, pp. 511-518, 1995

[15] A. B. Muller, "NEA Compilation of Chemical Thermodynamic Data for Minerals Associated with Granite", OECD/NEA, 1985

[16] R. J. Lemire and F. Garisto, "The Solubility of U, Np, Pu, Th and Tc in a Geological Disposal Vault for Used Nuclear Fuel", Atomic Energy of Canada Limited, AECL-10009, 1989

[17] I. G. McKinley, and D. Savage, "Comparison of solubility Databases Used for HLW Performance Assessment", *Fourth International Conference on the Chemistry and Migration Behavior of Actinides and Fission Products in the Geosphere*, pp. 657-665, 1994

[18] P. F. Salter and G. K. Jacobs, "Evaluation of Radionuclide Transport: Effect of Radionuclide Sorption and Solubility", *Scientific Basis for Nuclear Waste Management*, Vol. 11, pp. 801-810, 1982

[19] T. Yajima, Y. Kawamura, and S. Ueta, "Uranium (IV) Solubility and Hydrolysis Constants Under Reduced Conditions", *Scientific Basis for Nuclear Waste Management*, Vol. 353, pp. 1137-1142, 1995